JGR Atmospheres

RESEARCH ARTICLE
10.1029/2024JD041223

Differences in Thunderstorms' Ice Microphysics Between the Amazon and Central Africa Inferred From Spaceborne Passive Microwave and Radar Observations

Florian Morvais[1] and **Chuntao Liu**[1]

[1]Department of Physical and Environmental Sciences, Texas A&M University-Corpus Christi, Corpus Christi, TX, USA

Key Points:

- Amazonian systems are principally composed of smaller and more numerous ice crystals
- Increasing the Ice Water Content (IWC) and/or core size of thunderstorms in the Amazon demonstrates lower effectiveness in boosting lightning activity
- Amazonian systems present brightness temperatures unlike land or oceans but similar to oceanic regions with greater lightning activity

Correspondence to:

F. Morvais,
fmorvais@islander.tamucc.edu

Citation:

Morvais, F., & Liu, C. (2024). Differences in thunderstorms' ice microphysics between the Amazon and central Africa inferred from spaceborne passive microwave and radar observations. *Journal of Geophysical Research: Atmospheres*, *129*, e2024JD041223. https://doi.org/10.1029/2024JD041223

Received 22 MAR 2024
Accepted 14 AUG 2024

Author Contributions:

Funding acquisition: Chuntao Liu
Investigation: Florian Morvais
Methodology: Florian Morvais, Chuntao Liu
Supervision: Chuntao Liu
Writing – original draft: Florian Morvais
Writing – review & editing: Chuntao Liu

Abstract This study examines the differences related to microphysical properties of ice in thunderstorms over the Amazon and Congo Basin using the Precipitation Feature (PF) data sets derived from passive microwave and radar observations from the Tropical Rainfall Measuring Mission and Global Precipitation Mission Core Satellites. Analysis reveals that Amazon thunderstorms are likely composed of ice crystals smaller but more numerous than those in the Congo Basin, resulting in half as many flashes per PF on average in the Amazon, for similar Ice Water Content (IWC) or Area of 30 dBZ at −10°C (A_{charge}). The increase of the flash count following an increase of the IWC (A_{charge}) is only 72% (61%) as effective in the Amazon as it would be in the Congo Basin area. PFs with similar 30 dBZ radar echo top heights exhibit lower Brightness Temperatures (TBs) in the 85/89, 165, and 183 GHz frequencies over the Amazon, indicating more numerous smaller ice particles compared to those over the Congo Basin, which tend to show colder TBs at 37 GHz, possibly due to more numerous large graupel or hail particles. Comparisons of TBs in PFs with similar 30 dBZ echo top temperature between the Amazon and 3 × 3° global grids show that the median TB in Amazon is higher than that in most oceanic areas but is comparable to areas having high oceanic lightning activity (e.g., South Pacific Convergence Zone). It suggests that systems in the Amazon have similarities with maritime precipitation systems, yet with distinct characteristics indicative of land systems.

Plain Language Summary A comparison is made between Amazon (AM) and Congo Basin (CB) thunderstorms with similar reflectivity values seen by either TRMM or GPM, versus other variables that can help us understand the ice microphysics of these storms (IWC, area of 30 dBZ at −10C, Flash count, TBs). The radar reflectivity being driven by number and size (to the sixth power) of hydrometeors, the hypothesis is that for two storms with a same reflectivity value, one in AM and one in CB, the reflectivity value measured is driven by a higher concentration of large ice particles in CB (i.e., driven by size), while it is driven by a higher concentration of smaller ice particles in AM (i.e., driven by number). We quantify the lightning count difference between the two areas as a function of the amount of ice in the thunderstorm. It shows that AM produces significantly less lightning than CB on average for a similar ice content. Radiometers from TRMM and GPM are then used to compare the median TBs observed in the Amazon with the rest of the globe, to emphasize once again that AM is producing systems that are neither of land nor oceanic nature, but somewhere in the middle.

1. Introduction

It is well known that lightning occurs more often over land than over ocean (Christian et al., 2003; Orville & Spencer, 1979; Zipser et al., 2006). This is mainly because of the stronger updraft lifting, favoring larger ice particles, and consequently leading to an enhanced charge separation in continental convection compared to those over oceans (Cecil et al., 2005; Liu et al., 2012). Another reason could be the lower content in supercooled liquid water in oceanic clouds, an important factor that enables the separation of charges (Saunders & Peck, 1998; Takahashi, 1978). It is mentioned in Cecil et al. (2005) and yet to be validated, that the lower content of supercooled liquid water observed in oceanic clouds might result from lower cloud-base heights, hence depleting the available liquid water below the freezing level. Maritime systems are often characterized with weaker updrafts, in both width and speed (Williams & Stanfill, 2002), compared to their overland peers. The non-inductive electric charge separation mechanism is driven by interactions among the ice hydrometeors (i.e., graupel, hail, and cloud ice particles) and their environment (Gaskell, 1981; Saunders, 2008; Takahashi, 1978). Thus, a weaker updraft leads to a weaker inner-cloud electric field, and consequently to a lower flash rate.

With the development of satellite-borne lightning instruments (e.g., Optical Transient Detector (OTD; Boccippio, Goodman, & Heckman, 2000; Boccippio, & Koshak et al., 2000), Lightning Imaging Sensor (LIS) onboard of both the Tropical Rainfall Measuring Mission (TRMM; Albrecht et al., 2011) and the International Space Station (ISS; Blakeslee et al., 2020), and the consequent study of the global distribution of lightning, Central Africa appears to be the strongest lightning hotspot on Earth (Albrecht et al., 2016; Cecil et al., 2014; Zipser et al., 2006). Williams (2005) summarized the general lightning tropical chimneys (i.e., hotspots) as follows: "The ranking of these regions in lightning and rainfall now clearly indicate that Africa is the most continental chimney (most lightning, least rainfall), the Maritime Continent is the most maritime (most rainfall, least lightning), with the South American continent as intermediate." In an earlier work, Williams et al. (2002) qualified the Amazon rain forest as a "Green Ocean" due to pronounced similarities between Amazonian wet season (January-March) precipitation to that of oceanic systems, a description that is now widely used and accepted in the community.

Due to their contradictory behaviors despite being two similar areas (i.e., dominated by a tropical rainforest and a large river basin), the Amazon and the Congo Basin have often been compared together. For example, a large discrepancy in the rain amounts between the rain gauges and satellite retrievals over Africa suggest that convection in Africa occurs in a dryer environment (McCollum et al., 2000). It has been shown in many studies that the Amazon presents both lower frequency of occurrence of lightning storms and flash rates values compared to the Congo Basin (e.g., Boccippio, Goodman, & Heckman, 2000, Boccippio, & Koshak et al., 2000; Cecil et al., 2015; Futyan & Del Genio, 2007). Furthermore, a comparison made by Williams and Sátori (2004) shows that the surface of the Congo Basin exhibits a more continental profile than the Amazon (i.e., larger diurnal temperature range, larger Bowen ratio, stronger response to semiannual forcing, less inundation, lower boundary layer relative humidity, and slightly higher cloud base height). The Congo Basin is consequently more thermodynamically favorable to stronger updrafts and leads to greater lightning activity (Williams & Sátori, 2004). These findings follow the results of Nesbitt et al. (2000), which showed that African mesoscale convective systems (MCSs) tend to have maximum heights of 30-dBZ echo top between 1 and 2 km higher than South American ones. More importantly, the results of Williams et al. (2002) regarding the Amazon suggest that surface properties, although playing a major role, cannot be the sole reason for the oceanic-like regime observed in the Amazon.

To understand the physical mechanism of lightning in the thunderstorms over the two continents, it is important to examine the microphysics of ice in the convective cores, which are difficult to quantify, as *in-situ* observations cannot be collected due to aviation hazard. However, the existence of ice particles of large diameter (D) can be inferred from the radar reflectivity provided by ground-based radars by using the D^6 relationship in Rayleigh scattering (Wexler & Swingle, 1947). More importantly, radar reflectivity is a function of both size and number of hydrometeors, meaning that either a significant amount of small ice particles or fewer but larger ice particles could lead to the same reflectivity value. More information is needed to further constrain the ice microphysics.

Satellite passive microwave (PMW) observations are products that could provide additional information about cloud ice. They have been used as a proxy of convective intensity in the past (Mohr et al., 1999; Zipser et al., 2006). Microwave radiances emitted from land or liquid hydrometers are scattered by ice particles and lead to a depression of brightness temperature compared to the background seen by radiometers onboard satellites. Therefore, PMW radiances observed at the top of the atmosphere can be used to derive vertically integrated ice water path (Vivekanandan et al., 1991). Thanks to this relationship, they can also be linked to the lightning rate (Heuscher et al., 2022; Liu et al., 2011; Morvais & Liu, 2023).

In a two-part case study of Mesoscale Convective Systems (MCSs) at different life stages, Toracinta et al. (1996; part I) correlated higher flash rates in MCSs with smaller reflectivity lapse rates in the mixed-phase, while Mohr et al. (1999; part II) correlated the amount and distribution of lightning in MCSs to lower brightness temperature values at 85 GHz, due to scattering of the upwelling radiation by large ice particles.

Similarly, Liu et al. (2011) showed that the minimum brightness temperature value at 37 GHz is a good indicator of the probability of lightning in PFs, while their flash rate is more closely related to the area of low brightness temperatures. Liu et al. (2012) showed that the flash rate is better correlated with the area and volume of high radar reflectivity in the mixed-phase region than with proxies of maximum convective intensity. In addition to the lightning studies using ground-based radar observations by Deierling et al. (2008) and Deierling and Petersen (2008), it is generally accepted that the flash rate correlates better to the amount of ice within the mixed-phase region of the convective cores than it does to the maximum convective intensity of the thunderstorm. These

results concur with earlier works (Cecil et al., 2005; Zipser, 1994; Zipser & Lutz, 1994) that showed that a large ice mass in the mixed-phase region is important for lightning activity.

Through the use of either radar or passive microwave brightness temperatures, these studies emphasize the fact that lightning is closely related to the amount of ice within the mixed-phase region of thunderstorms. Although these studies linked lightning with either passive microwave or radar measurements, only a few studies combined both radar and passive microwave observations together to examine their relationships with lightning. For instance, Toracinta et al. (2002) related all three components (i.e., occurrence of lightning, maximum radar reflectivity, and minimum 85 GHz Polarization Corrected Temperature (PCT; Spencer et al., 1989)) to show that a similar ice scattering signature in different storms does not ensure a similar radar reflectivity response. Similarly, the relationship between the maximum reflectivity at 7 km and the minimum brightness temperature at 37 and 85 GHz PCT varies when related to the flash rate, as shown in Toracinta et al. (2002) and Cecil et al. (2002). It is observed that African thunderstorms tend to have lower brightness temperatures and higher flash rates than those in South American (Toracinta et al., 2002). Recently, Bang and Cecil (2021) presented composite radar reflectivity profiles for groups of storms that have a similar 20%–30% likelihood of hail (based on their passive microwave signal), which is consistent with very strong thunderstorms. For storms stratified by their 37 GHz PCT (Toracinta et al., 2002) depression, Amazonian storms appear to have a sharper decrease of reflectivity with height than Central African storms. For storms stratified by their 19 GHz PCT (Cecil & Chronis, 2018), storms in the Amazon exhibit higher reflectivity values at nearly all temperature levels compared to storms in Central Africa. These results highlight the importance of using both radar and PMW observations in the comprehension of the ice microphysics differences between the Amazon and Central Africa in order to better understand their differences lightning-wise.

Following this idea, this study first compares the thunderstorms of the Amazonian rain forest (AM) in South America with the ones in the Congo Basin (CB) area in Central Africa, easily considered to be the strongest lightning chimney on Earth. By comparing characteristics of thunderstorms between these two regions, we try to establish the hypothesis that thunderstorms with similar radar reflectivity profiles, but with different passive microwave ice scattering signals, would then have different ice particle sizes, which ultimately leads to differences in lightning rates. Then we apply this hypothesis around globe to compare it to the Amazon.

Specifically, this study attempts to answer the following questions:

- What are the fundamental differences in the ice microphysics of the thunderstorms in the Amazon versus Congo Basin?
- What are the lightning rate changes related to the different ice microphysics in these thunderstorms over two regions?
- What are the variations of ice microphysics in deep convective clouds around the globe in comparison to the Amazon?

This study is organized following three sections. Section 2 introduces the data, methodology, and hypothesis. The results are presented in Section 3, with two main objectives. The first goal is the direct comparison between properties of thunderstorms from the Amazon area and Congo Basin to infer ice microphysical differences, while the second one aims to compare the Amazon region with the rest of the world using satellite passive microwave brightness temperature observations. The major conclusions are summarized in Section 4.

2. Data and Methods

2.1. Precipitation Features Database

To describe the properties of thunderstorms, the Precipitation Features (PFs) database (Liu et al., 2008), including the properties of precipitation systems observed by the Tropical Rainfall Measuring Mission (TRMM) satellite, as well as the Global Precipitation Mission Core Satellite (GPM) are used in this study. Both data sets rely on the Ku-Band precipitation radars aboard their respective satellites to define the PFs: the Precipitation Radar (PR; 13.8 GHz) for TRMM, and the Dual-Frequency Precipitation Radar (DPR; Ku in 13.6 GHz and Ka in 35.5 GHz (the Ka band data are not used in this study)) for GPM. In both data sets, PFs are defined as at least 4 contiguous pixels of near surface precipitations (i.e., at least ~71.8 km^2 (or 81.4 km^2 after boost in 2001) for TRMM, and ~98.2 km^2 for GPM), as derived from the Ku band radar reflectivities at the near surface. Each PF is consequently an object with known time, location, and precipitation area, allowing an easy collocation with other observational

and model generated variables. Note that only precipitating clouds are considered in these data sets. Any features with a precipitation area lower than four pixels or a precipitation rate lower that the detection capabilities of the precipitation radar instruments (i.e., ∼0.1 mm/hr) are excluded. Lightning may occur in PFs with sizes less than four pixels (∼0.27% in tropics), and sometimes even occur in cloud areas without surface precipitation (∼5.5% in TRMM domain (Peterson & Liu, 2011). These scenarios are not considered in the following discussion.

In the case of this study, the TRMM-PFs data set ranges from 1998 to 2013, and the GPM-PFs data set ranges from 2015 to 2021. Only full years (i.e., full 12-month, from Jan. to Dec.) of data are used to ensure full seasonal sampling, hence the non-usage of the fully available data. Additionally, data in 2001 are excluded from the TRMM-PFs data set since the orbit height of the satellite increased from 350 to 403 km during the month of August, introducing a gap in the data. Note that the change in pixel area is considered in the computation of the precipitation area used later on in this study (i.e., 17.96 km^2/pxl before vs. 20.35 km^2/pxl after orbit boost for TRMM; Liu et al., 2008).

The PF database consists of numerous variables, from both observational and modeling origins. In the specific scope of this study, for a microphysics comparison with a lightning focus, the properties used are summarized as follows: longitude and latitude representing the location of the geo-center of the PF object; year, month, day, and hour (as a float value) representing the time of occurrence; the Ku band radar reflectivity corresponding to the maximum reflectivity observed at altitudes of 0.5 km interval; the Ice Water Content (IWC; integrated through the entire PF area) and the area of 30 dBZ at −10°C as products of the reflectivity measurements; and the minimum value of the Brightness Temperature (TB) measured by the radiometers on board of TRMM (i.e., TRMM Microwave Imager (TMI) at 37 and 85 GHz) and GPM (i.e., GPM Microwave Imager (GMI) at 37, 89, 166, and 183 GHz) to further explore the inner content of the clouds. Here the radar profiles at different heights are linearly interpolated to the specific temperature levels using the collocated temperature profiles from the ERA5 reanalysis data (Hersbach et al., 2020). The IWC is estimated using the simple reflectivity to mass relationship from Carey and Rutledge (2000). Additionally, the TRMM-PFs data set includes the lightning rates observed by the Lightning Imaging Sensor (LIS; Christian, 1999) on board of TRMM, allowing a comparison of Precipitation Features with Lightning (LPFs; TRMM-LPFs) within it.

2.2. Methodology and Hypothesis

The strength of thunderstorms is commonly assessed using radar reflectivity (Wexler & Swingle, 1947; Zipser & Lutz, 1994). It has been established that the power received by the radar scattered back by a cloud is driven by the number of particles and their diameter to the sixth power following the Rayleigh law of scattering when radar wavelength is much larger than the particles (Wexler & Swingle, 1947). The logarithmic scale of the reflectivity is used as a consequence of the strong impact that a small increase in particles radius has on its value.

On the other hand, the passive microwave radiometers using frequencies ranging from 37 to 183 GHz have wavelengths ranging respectively from 0.81 to 0.16 cm. Such wavelengths are proportional to the diameter of large ice particles and are falling within the scope of the Mie scattering theory. As seen in Mroz et al. (2017), which calculates the extinction coefficient of spherical hailstones as a function of the diameter at the GMI frequencies (Mroz et al., 2017, Figure 6b). Following their results, the peaks of extinction of the channels range from approximately 0.2 cm for 166 GHz and 0.6 cm for 37 GHz. The scattering of microwave radiances by ice particles at these frequencies has variable exponential relationships to IWC in cloud (Vivekanandan et al., 1991). In general, the strength of scattering can be expressed as exponential function of IWC with power ranging from 1.1 at 85 GHz to 1.6 at 37 GHz, although Mie scattering cannot realistically fully describe the interaction between the microwave signal and non-spherical ice particles. At higher frequencies, the passive microwave brightness temperatures can be expressed as exponential functions to the ice water path with power values even lower than those (Wu, 1987).

Therefore, compared to the sixth power relationship of the ice particle size from radar reflectivity at lower frequencies, passive microwave radiance depression by ice scattering at higher frequencies is relatively less sensitive to the larger ice particles with sizes comparable to the radiance wavelengths due to the Mie scattering. This means that for two systems with a similar radar reflectivity vertical structure, the one with a stronger ice scattering signal (i.e., colder TB) would have relatively smaller, but more numerous ice particles than the one with a weaker ice scattering signal (i.e., warmer TB). Because the in-cloud electrical charge separation is directly related to the amount of large ice particles colliding with the abundant supply of smaller ice crystals in an environment filled

with supercooled liquid water (Gaskell, 1981; Saunders, 2008; Takahashi, 1978), for two systems with a same radar reflectivity, we hypothesize that the one with colder TBs would have relatively less lightning than the one with warmer TBs.

By taking advantage of the different physical processes leading to radar reflectivity observations (driven principally by Rayleigh scattering from hydrometers mostly having size much smaller than the radar wavelength) versus passive microwave radiometer brightness temperatures (driven principally by Mie scattering due to microwave wavelengths comparable to hydrometeor sizes) and the above hypothesis of ice particle size versus TB for similar radar reflectivity, this study attempts to propose an explanation as to why two similar storms reflectivity-wise, one over the Amazon and the second over the Congo Basin, would have significantly different lightning activity. We attempt to show that thunderstorms over the Amazonian rain forest must have smaller ice particles than those in Congo Basin in general.

3. Results

3.1. Global Distribution of Thunderstorms and Their Radar Echo at −10°C

The geographical distribution of samples of TRMM-LPFs on 2 × 2º grid is shown in Figure 1a. As mentioned earlier, South America, Central Africa, and Maritime continents appear as lightning chimneys (Williams, 2005). There is a slight increase of LPF samples north/south of 30°N/30°S due to the oversampling resulting from the curve of the satellite orbit. Although South America and Central Africa are both lightning hotspots, Figure 1b shows that the probability of having lightning in a PF is higher in CB (i.e., approximately 13%–23%) than it is in AM (i.e., below 10%). The fraction of TRMM-LPFs having a maximum echo top height of 30 dBZ reaching temperatures colder than −10°C is presented in Figure 1c. Data show consistently around the globe (i.e., when above 20 samples) that above 90% of TRMM-LPFs meet the maximum height of 30 dBZ reaching temperatures colder than −10°C threshold observed by Liu et al. (2010) (i.e., about 10% of PFs have lightning when their 30 dBZ echo top temperature is around −10°C for land or −17°C for oceans). Note that the colormap used in Figure 1c goes from 80% to 100% while values are as low as 57%. Values at and lower than 80% are consequently not shown. This choice was made to enhance the visibility of the map. Due to the South Atlantic Anomaly, a lower fraction of LPFs are found near the lower southeast coast of South America and result from a higher sensor false alarm in the area (Pechony & Nickolaenko, 2010). The fraction of TRMM-LPFs with a maximum echo top height of 40 dBZ reaching temperatures colder than −10°C observed in Figure 1d shows a drastic contrast in lightning activity between AM and CB. Only approximately 50%–65% of the TRMM-LPFs have 40 dBZ reaching −10°C in CB while less than 40% do in AM. Hence the choice of comparing the AM with the CB. This difference implies that most Amazonian storms are lacking in either number or size of ice particles to reach 40 dBZ at higher altitudes.

Central Africa has been shown through satellite observations to have a strong hail signature in both PMW (e.g., TRMM-TMI and GPM-GMI in Bang & Cecil, 2019) and radar reflectivity (e.g., GPM-DPR in Mroz et al., 2017; Le & Chandrasekar, 2021) but lacks ground validation to be defined as a hail hotspot. However, it is suspected that the strong hail signature observable in Central Africa may not translate as large hail reaching the ground. For example, it is suggested that hail is more likely to melt on its way down in the tropics (Allen et al., 2020; Brook et al., 2024). A higher tropopause in the tropics may support deeper layers of ice, further decreasing the brightness temperature measured and being identified as hail signature. Bang and Cecil (2019) showed that although being at similar latitude, AM did not show a strong hail signature. At minima, CB tends to present higher contents in large hydrometeors aloft compared to AM. By comparing similar LPFs over AM and CB, this study aims to show that thunderstorms in the two regions tend to have different particle size distributions: larger particle sizes in smaller concentrations in CB, and smaller particle sizes in larger concentrations in AM. To achieve this goal, this study compares AM storms with CB ones by exploring their respective relationships between radar reflectivity properties (e.g., maximum reflectivity, IWC, area of 30 dBZ at −10°C, and maximum height of 30 dBZ) and parameters related with the properties of ice particles (e.g., flash count and passive microwave TBs), hence confronting the radar similarities between PFs of the two regions with their differences in hydrometeor content. Note that both the AM and CB data are selected within the boxes shown in Figure 1 (i.e., 75ºW–60ºW, 10ºS–5ºN for AM; 15ºE–25ºE, 15ºS–5ºN for CB). This leads to a sample size of 26,875/30,224 for TRMM-LPFs and 106,916/48,168 for GPM-PFs over AM/CB. Here we avoid elevated regions (e.g., Andes in South America or the

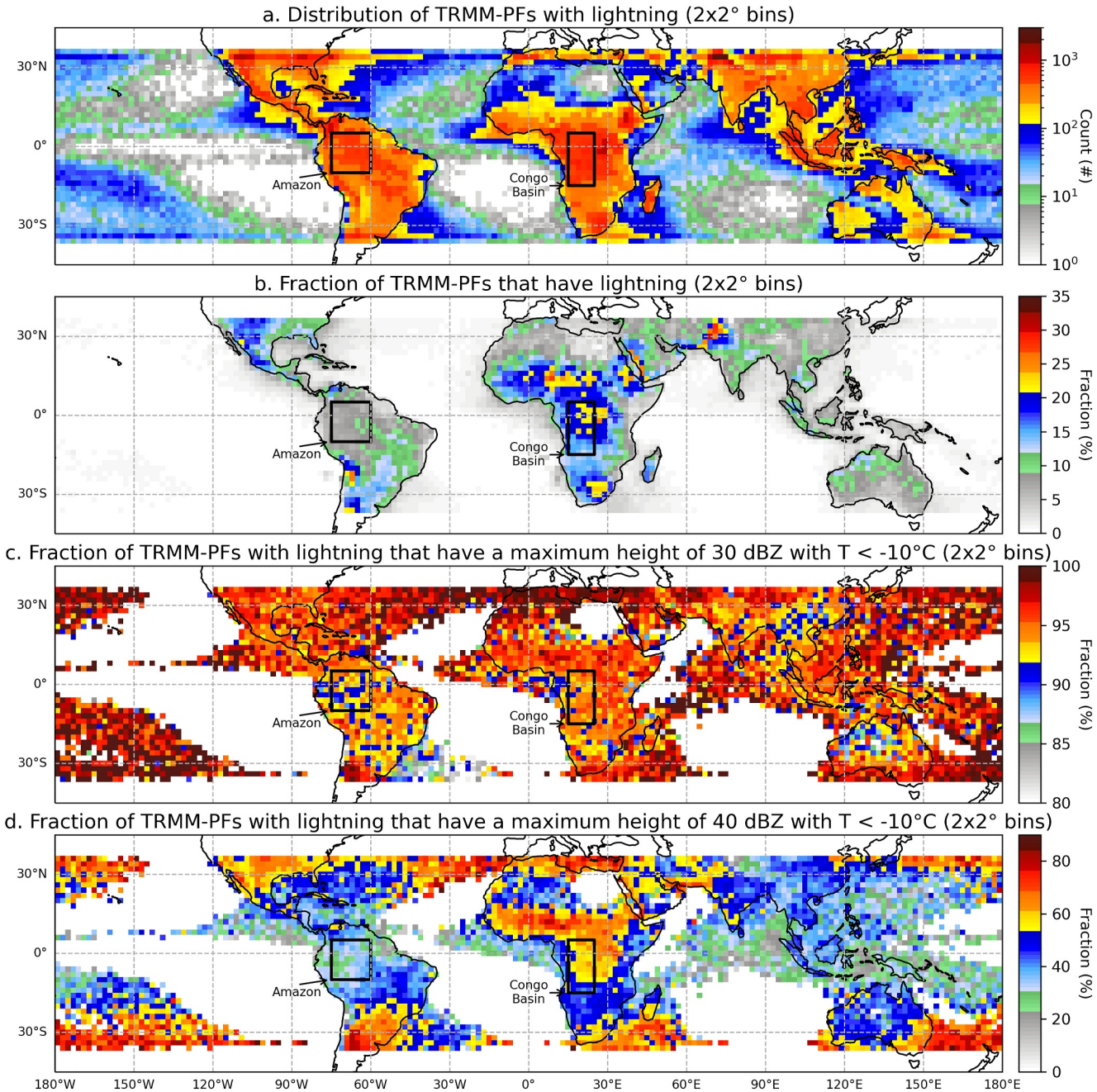

Figure 1. Geographical distribution of the population of (a) Lightning PFs (LPFs), with (b) the fraction of PFs having lightning, (c) the fraction of LPFs with a maximum height of 30 dBZ reaching temperatures colder than −10°C, and (d) the fraction of LPFs with a maximum height of 40 dBZ reaching below −10°C in 1 × 1° bins. The Amazon box is (75°W–60°W, 10°S–5°N) and the Congo Basin box is (15°E–25°E, 15°S–5°N). Fractions are not shown for grid cells with a sample size inferior to 20. The TRMM-PFs data range from 1998 to 2013.

Great Rift Valley in Central Africa) where cloud to ground lightning is enhanced due to high ground (e.g., Boccippio et al., 2001; Murphy & Nag, 2015).

3.2. Altitude Versus Reflectivity

The normalized Cumulative Frequency by Altitude Diagrams (CFADs) of maximum reflectivity in LPFs over AM (a), CB (b), and their difference as AM—CB (c) are presented in Figure 2. Each of the 40 horizontal altitude levels is normalized horizontally, creating unique 1D-histograms adding-up to 100%. This normalization at each

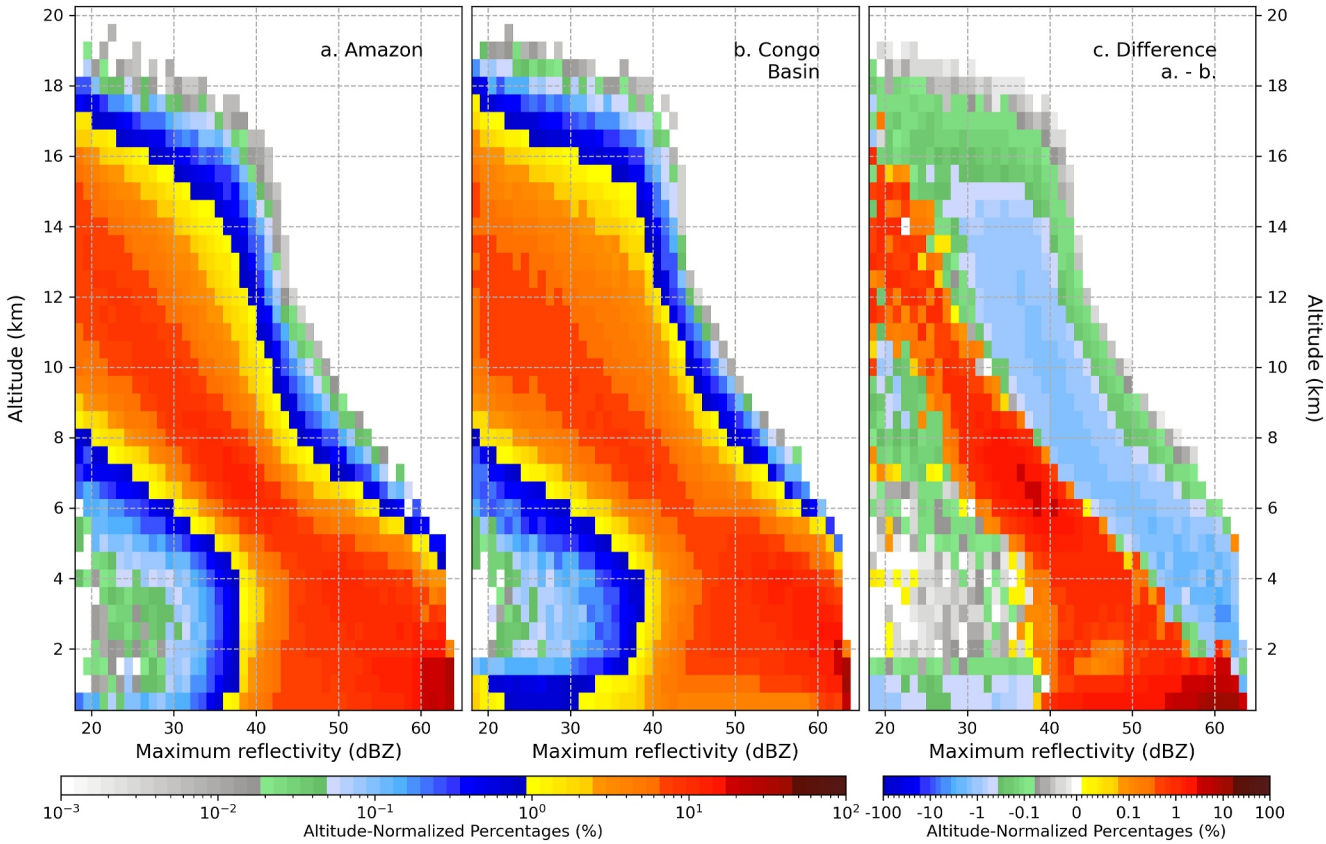

Figure 2. Cumulative Frequency by Altitude Diagram of TRMM maximum Ku radar reflectivity in TRMM-LPFs for (a) AM, (b) CB, and (c) difference between (a) minus (b). Values are normalized at each altitude level (i.e., each altitude level adds up to 100%). The TRMM-PFs data range from 1998 to 2013.

y-axis level is used in all the following 2D-histograms (Figures 2–5). Figures 2a and 2b show that the distributions of the maximum of reflectivity profiles for AM and CB are in general similar, having a decreased maximum reflectivity with altitude. A significant decrease of reflectivity at around 4.5 km is related to the refractive index property transition from liquid rain drop to solid ice particle. However, CB has higher reflectivity values than AM in general. This is clearly shown in the difference of the two regions in Figure 2c.

Interestingly, the difference between AM and CB CFADs appears to have a tri-pole structure: (a) higher maximum reflectivity values are more frequently observed in CB, (b) lower maximum values are more often observed in CB as well, and (c) the in-between values are more prevalent in AM. The results infer that CB has a broader distribution of reflectivity values, which could result from the degree of abundance or absence of large hydrometeors in the cloud. AM however has a narrower distribution of maximum reflectivity values, which seems to support the hypothesized lower content in large hydrometeors and abundance of small ice crystals. Because reflectivity is more sensitive to the size of the hydrometeors (i.e., to the sixth power), a large fluctuation in quantity of small hydrometeors would be needed to significantly affect the maximum reflectivity observed.

3.3. IWC and Area of 30 dBZ at −10°C Versus Flash Count

An alternative to show the difference between AM and CB LPFs is to explore the relationships between radar reflectivity properties and lightning counts. Figure 3 presents the normalized 2D-histograms, where the LPFs lightning flash counts in the two regions are compared to their total IWC and Area of 30 dBZ at −10°C (A_{charge}). The Area of 30 dBZ at −10°C provides a good approximation of the size of the core of the storm, which is known to be well correlated with flash count (Laksen & Stansbury, 1974; Liu et al., 2011).

It is clear that LPFs with higher values of IWC or A_{charge} have more flashes. Lightning is the natural phenomena that allows the neutralization of a portion of the charges accumulating within different areas of the cloud (or with

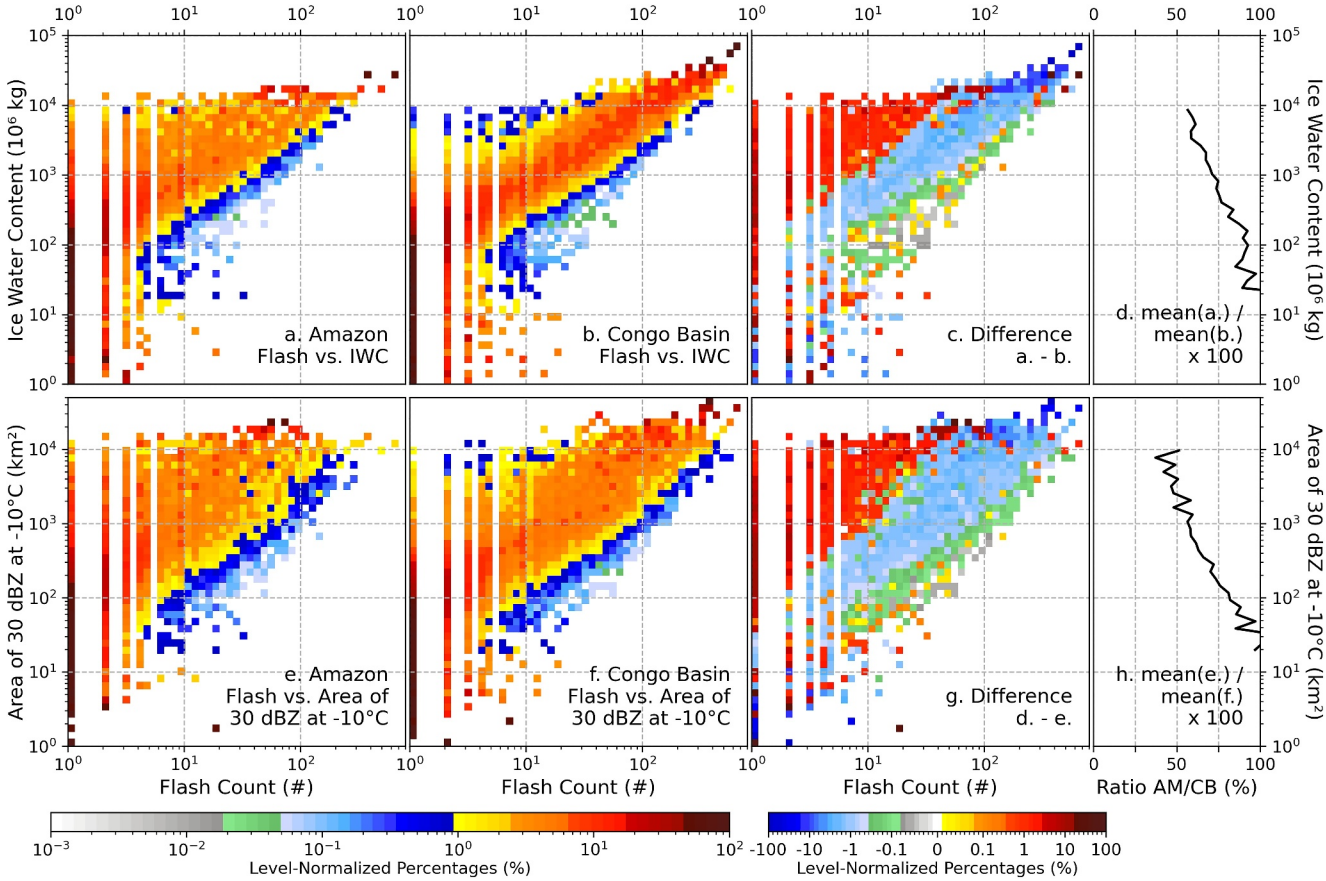

Figure 3. Normalized two-dimensional histogram of TRMM LPFs as function of Flash Count versus Ice Water Content (IWC) for (a) AM, (b) CB, and (c) difference between (a) minus (b). The ratio of the mean flash count observed in AM divided by the mean flash count observed in CB, as a percentage, is represented in panel (d). The relation between Flash Count and Area of 30 dBZ at −10°C (A_{charge}) is represented in a similar way in plots (e, f, g, and h). Values are normalized at each IWC and Area level (i.e., each IWC or Area level adds up to 100%). The TRMM-PFs data range from 1998 to 2013.

the ground). It consequently requires the presence inside the cloud of an electric field strong enough to initiate the electric spark. However, such a strong electric field requires in-turn a strong charges separation mechanism, which relies on interactions between small and big hydrometeors within the cloud. Consequently, a higher flash count can be resulted from either a large area with a strong electric field, or a rapid charging of the cloud layers to counteract the dissipation of the electric field (due to each individual lightning flash), or a combination of both. Therefore, a high flash rate implies plentiful collisions among large, riming graupel and smaller ice particles, which can be proxied with both Ice Water Content and A_{charge}. Note that the narrower 2D distributions of the data over the CB (Figures 3b and 3f) compared to AM (Figures 3a and 3e) implies a stronger correlation of the lightning count with IWC and A_{charge} in CB.

There is a shift in the distributions, data show that for any value of either IWC or A_{charge}, the CB region has higher probabilities to produce more lightning flashes (Figures 3c and 3g). For example, Figure 3c shows that for a total IWC of $10^3 \times 10^6$ kg, AM LPFs have a higher probability to produce less than 10 flashes while CB LPFs are more likely to produce over 10 flashes, up to a hundred. Similarly, Figure 3g shows that for an A_{charge} of 10^3 km^2, a higher proportion of AM LPFs produce low flash counts (i.e., below 10) while a higher proportion of CB LPFs produce higher flash counts (i.e., 10–100 flashes). The TRMM-LPFs data set clearly shows that for a similar IWC or A_{charge}, CB produces significantly more lightning than the AM.

These lightning generation differences over the two regions are quantified in Figures 3d and 3h. It is defined as the LPFs' mean flash count in AM divided by that in CB, for each specific IWC and A_{charge} level, and reported as a percentage. The results are shown only when the sample size is sufficient (i.e., above 100 samples in both AM and CB) to provide a trustworthy noise-less result. For a similar IWC or A_{charge} value, AM tends to produce

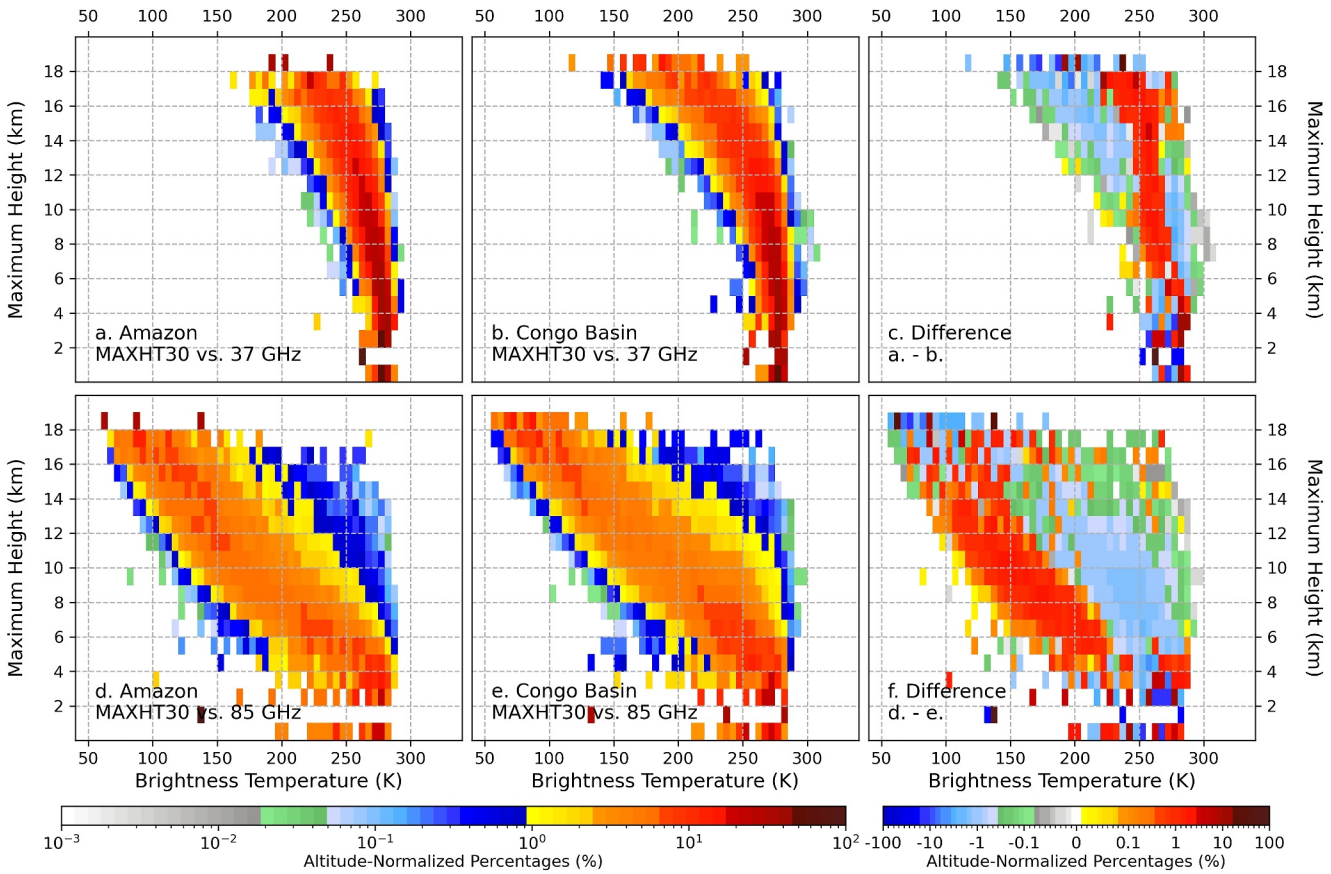

Figure 4. Normalized two-dimensional histogram of TRMM-LPFs as function of the Maximum Height of 30 dBZ versus Minimum Polarization Corrected Brightness Temperatures (PCT) at 37 GHz for (a) AM, (b) CB, and (c) difference as (a) minus (b). Similarly, panels (d, e, and f) show the relationship for 85 GHz PCT. Values are normalized at each altitude level (i.e., each altitude level adds up to 100%). The TRMM-PFs data range from 1998 to 2013.

significantly less lightning. This difference increases with the IWC or A_{charge} value, and reaches twice as many flashes observed in CB compared to AM for the higher values of either IWC or A_{charge}. In CB, an increase of the IWC or Area of 30 dBZ at −10°C translates as a significant increase in flash count. In AM, there is a weaker increase of the flash count compared to CB when the IWC or Area of 30 dBZ at −10°C values are increasing.

To quantify the efficiency of the translation of an increase of IWC or A_{charge} toward an increase in lightning, the ratios for IWC and A_{charge} are computed as the sum of the lightning flash counts divided by the sum of the IWC and A_{charge} respectively. The results for AM and CB are presented in Table 1. These ratios are then used to directly compare the two areas together through the ratio between AM and CB. On average, an increase of the lightning count following an increase of the IWC in AM is only 72% as effective as it would be in CB, and an increase of lightning against the A_{charge} in AM is only 61% as effective as it would be in CB.

In studies made by Petersen and Rutledge (2001) and Petersen et al. (2005), it is suggested that when considered on a global scale, the relationship between the amount of ice and the lightning flash density is invariant between land, coastal, and oceanic regimes. Although it is shown that the three regimes display differences in the slopes of their lines of best fit below ∼20% (Petersen et al., 2005), it is important to note the large spread of values around it. It implies that although the average ice content versus lightning relation might be consistent around the globe, local influences persist, as shown in Figure 3. There is a significant difference in lightning count for storms of similar ice content over AM compared to CB. The hail climatology made by Bang and Cecil (2019) in the GPM domain shows that Central Africa is a hail hotspot candidate (i.e., needs ground validation) while the Amazonian rain forest shows little hail occurrence. Note that the ice content proxies (i.e., IWC and A_{charge}) used in Figure 3 are not direct measurements but are estimated from the spaceborne radar reflectivity measurements (i.e., IWC is integrated from the reflectivity profiles through the entire PF area and A_{charge} is the area of 30 dBZ at −10°C). The

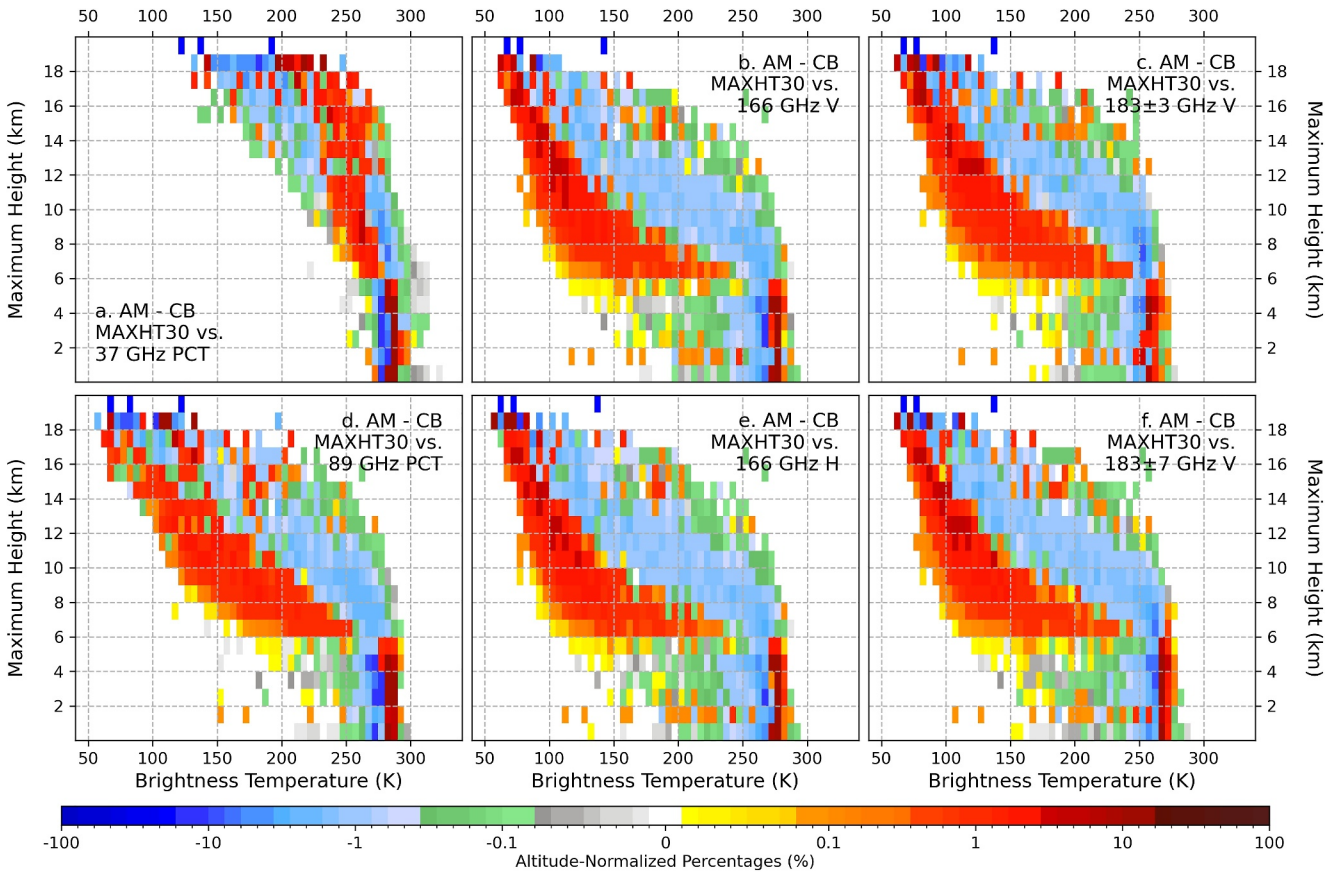

Figure 5. Difference between the normalized two-dimensional histograms of GPM-PFs with 30 dBZ echo top colder than −10C as function of the Maximum Height of 30 dBZ versus Brightness Temperatures over Am and that over CB. Similar to Figure 4d, except differences are shown as AM minus CB for (a) 37 GHz PCT, (b) 166 GHz Vertical, (c) 183 ± 3 GHz Vertical, (d) 89 GHz PCT, (e) 166 GHz Horizontal, and (f) 183 ± 7 GHz Vertical. The GPM-PFs data range from 2015 to 2021.

calculation is consistent for all PFs through the entire domain without considering the variation of reflectivity versus ice mass relationship. Considering that this work aims to show that the Amazon hydrometeors' distribution is balanced around smaller and more numerous ice crystals, while the Congo Basin hydrometeors' distribution is balanced around bigger and less numerous ice crystals, it is expected that the derived IWC might be underestimated in AM and overestimated in the CB. Nevertheless, it is possible to use the lightning initiation theories to hypothesize the following:

- In the Congo Basin, an increase of the ice content may come from an increase in the concentration of large ice particles within the cloud. It can lead to radar reflectivity values higher than 40 dBZ (Figure 1d), and an enhancement of the charge separation mechanism, which is introduced by large ice particle collisions from terminal velocity differences, and consequently to a significant increase in lightning flash count (Figure 3).
- In the Amazon, an increase of the ice content may come from an increase in the concentration of small ice particles within the cloud. It consequently may not translate into a significant increase of the radar reflectivity values (Figure 1d), and would not enhance significantly the charges separation without a significant increase in the concentration of large ice particles, and consequently do not significantly increase the flash count (Figure 3).

Table 1
Mean Lightning Counts per IWC and Area With 30 dBZ at −10°C (A_{charge}) From LPFs in AM and CB

	AM	CB	AM/CB
flash/IWC (#.10^{-6}.km^{-2})	0.901×10^{-2}	1.244×10^{-2}	0.72
flash/A_{charge} (#.km^{-2})	0.946×10^{-2}	1.553×10^{-2}	0.61

Note. The right column lists the ratios between two regions.

3.4. Maximum Height of 30 dBZ Versus Brightness Temperatures

Passive microwave brightness temperatures observed at the top of the atmosphere are the products resulting from the Earth's upwelling microwave radiance being affected by the atmosphere and by a cloud's hydrometeor

content. Each passive microwave frequency is chosen, within the atmospheric absorption window, for its sensitivity to a slightly different process within the cloud, hence providing an insight of a cloud's inner content.

It has been shown that radiances at 37–86 GHz are significantly affected by ice in the cloud and are interesting proxies for IWP (Adler et al., 1991; Smith et al., 1992; Vivekanandan et al., 1991). Although Mroz et al. (2017) show that for GPM, the 19 GHz channel (i.e., extinction coefficient peaks between 1.0 and 1.5 cm; 19 GHz has a wavelength of ∼1.58 cm) is more sensitive to large hail than the 37 GHz channel (i.e., extinction coefficient peaks around 0.6 cm; 37 GHz has a wavelength of ∼0.81 cm), it is shown in Cecil (2009) that 37 GHz is more suitable for large hail observations in TRMM data, with TRMM-PFs having 70% likelihood of being associated with hail reports when below 180 K. The difference can be assumed to result from the wider footprint of TRMM's TMI, leading 37 GHz to appear as the best tradeoff between lower frequencies being desirable for distinguishing larger versus smaller particles, and higher frequencies having better spatial resolution. Additionally, sufficient concentrations of graupel have been shown to be observable at 37 GHz as well, even in the absence of hail (Leppert and Cecil, 2015, 2019). Studies suggest that a channel around 150 GHz is a good candidate to observe frozen precipitation in middle and high latitudes (Bennartz & Bauer, 2003; Michele & Bauer, 2006), and the G-band (i.e., 183 GHz) is known to be extremely sensitive to changes in water vapor (Bennartz & Bauer, 2003; Racette et al., 2005). Note that most frequencies are well correlated with several different hydrometeors within the cloud (Mech et al., 2007) and are hence impacted by multiple different processes within the cloud.

The relationship between Maximum Echo Top Height of 30 dBZ (MAXHT30) and Brightness Temperatures is shown in Figures 4 and 5. TRMM-LPFs (i.e., only PFs with lightning) are presented in Figure 4, which shows the relationships with 37 GHz PCT (top row) and 85 GHz PCT (bottom row). The left panels represent AM, the center panels represent the CB, and the right panels show the difference as AM minus CB. Similarly, the relationship between MAXHT30 and Brightness Temperatures for the GPM-PFs (i.e., all PFs) data set is presented in Figure 5, where only the differences (i.e., AM minus CB) are shown, including 6 different GPM GMI channels. In both figures, data are normalized along the TBs for each altitude-level.

Figure 4 shows that both regions present a similar relationship between MAXHT30 and 37 and 85 GHz: higher values of MAXHT30 are correlated with lower brightness temperatures, with a clear trend in the 85 GHz channel but a weaker reaction from 37 GHz to MAXHT30 changes. For any specific value of MAXHT30, CB has a broader distribution with higher fractional occurrence at both the lower (down to ∼100 K) and higher (up to ∼300 K) TB values in the 37 GHz frequency. AM has a narrower TB range in brightness temperatures (∼230–270 K). In the 85 GHz frequency, the spreads are reversed with AM having more of lower TB values and CB having more of higher TB values. These results are in agreement with the GPM-PFs data shown in Figures 5a and 5d.

If we make an assumption that 37 GHz is mainly driven by large hydrometeors and 85/89 GHz by the integrated IWP, these results agree with the previously hypothesized theory. At 37 GHz, the broader distribution of TB values in CB may be due to a greater variability of the number of large hydrometeors, while the narrower spread for AM may be resulting from a significantly lower, and more consistent, content in large particles. At 85/89 GHz, AM tends to have lower TBs, leading to the implication that despite having a lower content in large ice particles, AM PFs have a higher integrated ice water mass than those over CB. This is consistent with the hypothesis that AM precipitation systems are composed of a larger proportion of smaller hydrometeors. This statement is also supported by the results from higher frequencies shown in Figures 5b–5f, where convective systems over AM have a distribution of their TBs that peaks lower for any given 30 dBZ echo top. If we make the assumptions that TBs at 166 and 183 GHz channels are principally correlated to frozen precipitation, it consequently implies a higher ice water content in AM compared to CB, likely from numerous smaller particles compared to those over the CB.

3.5. Comparison of the Amazon With the Globe

Using AM as a reference (i.e., 75°W–60°W, 10°S–5°N), the median TB value of each channel is computed around the globe in a 3 × 3° grid, with a filtering between −17°C and −10°C for the temperature at echo top height of 30 dBZ (T_{30dBZ}) following Liu et al. (2010). Hence, using only the selected samples, Figures 6–9 show the differences between the median brightness temperature values within the 15 × 15° AM box and the local (i.e., 3 × 3° grid boxes) median values for each frequency channels from TRMM and GPM. The median TB values inside the AM box for each of the different channel frequencies are summarized in Table 2.

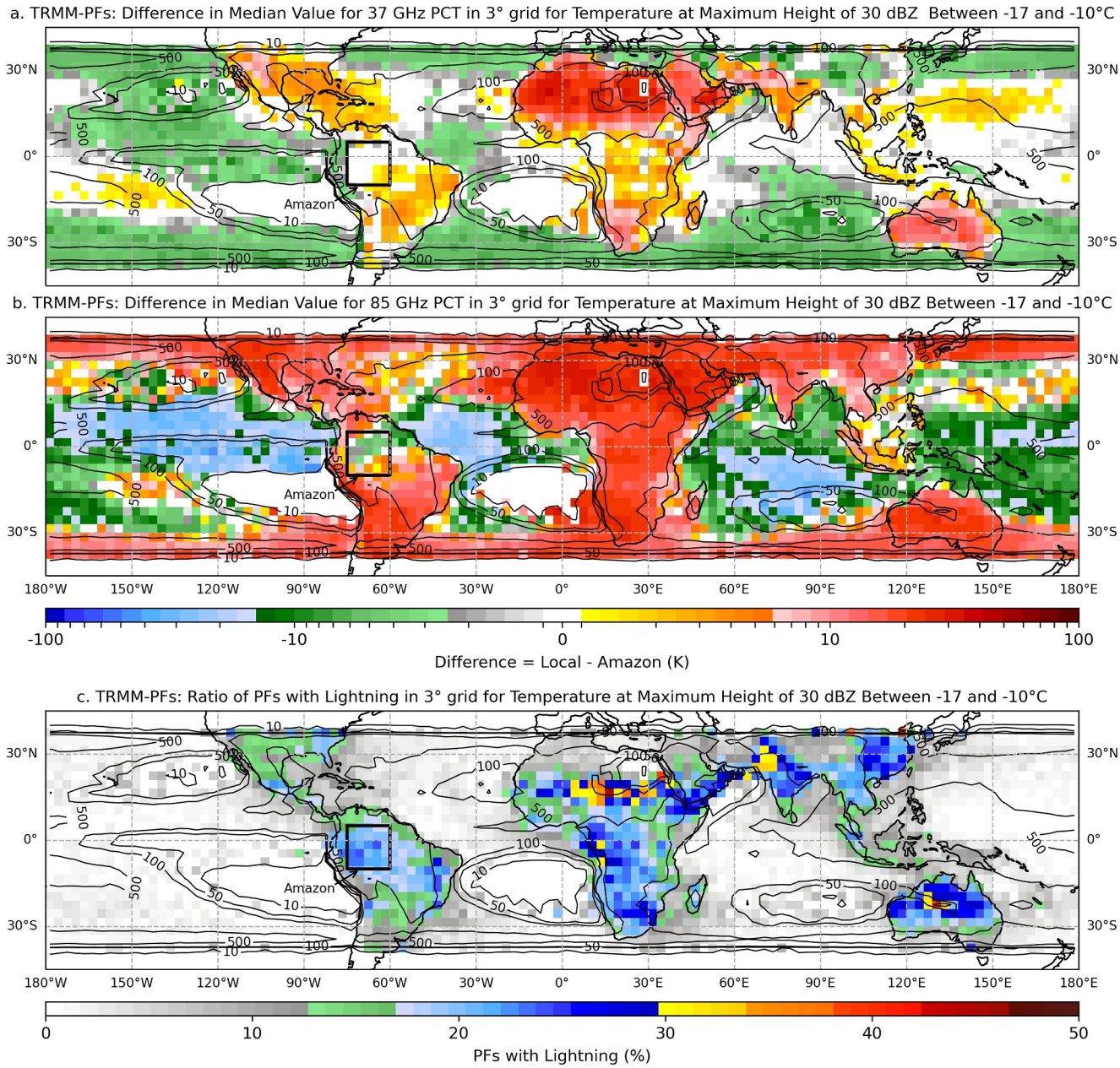

Figure 6. Difference in median TB between the local 3 × 3º grid and the 15 × 15° Amazon box for TRMM-PFs with T_{30dBZ} between −17°C and −10°C for (a) 37 GHz PCT, and (b) 85 GHz PCT. Panel (c) presents the proportion of PFs observed to have lightning activity by TRMM-LIS. Sample size is presented by the black contours. The TRMM-PFs data range from 1998 to 2013.

The filtering (i.e., between −17°C and −10°C for the temperature at maximum height of 30 dBZ) is based on the results of Liu et al. (2010). Their study shows that T_{30dBZ} values of −10°C (land) and −17°C (oceans) are roughly corresponding to 10% occurrence of lightning in precipitation features (i.e., approximately 10% of PFs have lightning). This value range has been chosen to examine systems marginally having lightning. At colder value ranges, similar results are found (Figures not shown). Note that the PF database used in this study is slightly different from the PF database used in Liu et al. (2010) (e.g., use of full years of data, more years of post-boost data, and a different reanalysis product). This leads to slightly different lightning percentages. For example, using land PFs with T_{30dBZ} between –9°C and −11°C, only 7.5% of them are having lightning, which is lower than 10% (Table 3). Although the Ku-band frequencies used by both TRMM-PR (13.8 GHz) and GPM-DPR (13.6 GHz) are nearly identical, the slightly different field of view and vertical sampling between the two radars could also have

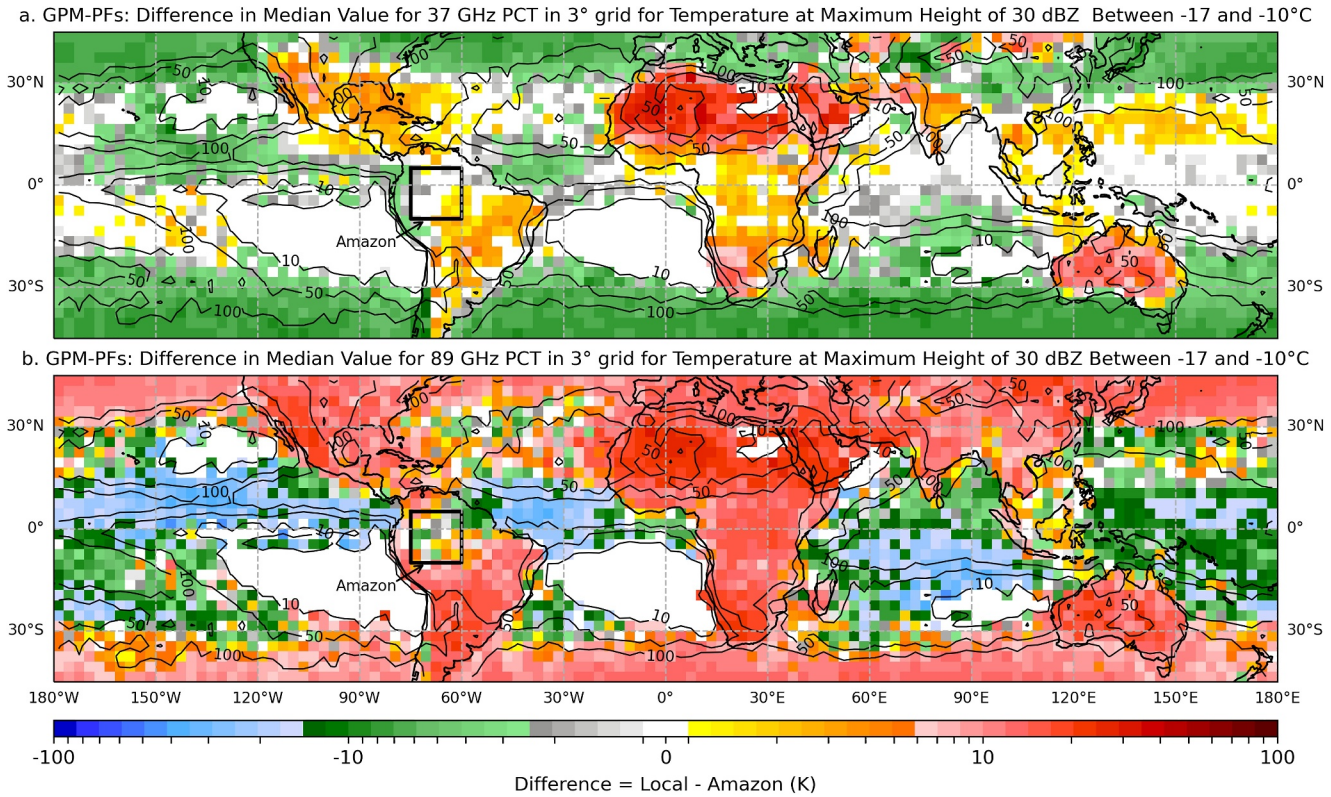

Figure 7. Same as Figure 6, except for GPM-PFs, with (a) 37 GHz PCT, and (b) 89 GHz PCT. The GPM-PFs data range from 2015 to 2021.

influences in the 30 dBZ echo top heights. However, this study focuses on the regional comparisons from each satellite. The same T_{30dBZ} criteria used for both TRMM and GPM would only have a slight difference in the selection of samples.

The results presented in Figures 6–9, as the subtraction of the local median TB value minus the AM median TB value, show the differences from the local TB median to the AM TB medians listed in Table 2. Positive values in warm colors are showing that the median is higher in the local grid box than it is in AM, suggesting a stronger ice scattering signal in AM. On the opposite side, negative values in cool colors mean that the median is lower in the local grid box than it is in AM, inferring a stronger ice scattering signal in the local grid box.

At 37 GHz (Figure 6a for TRMM-LPFs and Figure 7a for GPM-PFs), AM has higher TB values than the ocean and slightly lower compared to other land regions. It implies that 37 GHz radiance is further attenuated in convection over the oceans than it is over land for PFs with T_{30dBZ} between −17°C and −10°C. Although this result seems contradictory with the assumption that 37 GHz is driven by large hydrometeors (and consequently should have lower values over most continents), it results from the complexity of brightness temperatures, which have been shown to be correlated with several different types of hydrometeors (Mech et al., 2007). Note that the emission from liquid water (i.e., mostly coming from liquid rain drops, with supercooled liquid water having a small contribution (Wilheit et al., 2006)) may also slightly contribute to the observed warm TBs at this frequency.

At 85/89 GHz (Figure 6b for TRMM-LPFs and Figure 7b for GPM-PFs), AM has higher TB values than the ocean but lower values than land. It implies that oceanic systems may be composed of a higher ice water content in the form of smaller hydrometeors than land, with AM systems being in the middle. At 166 and 183 GHz (Figures 8 and 9), AM has higher TB values than the ocean but significantly lower values than land. This would imply that the frozen particles contents are significantly higher for oceanic PFs than they are for land PFs, with AM PFs being in-between.

These results tend to align with the "Green Ocean" description of AM. Note that "Green Ocean" (Williams et al., 2002) characterizes the similarities of the Amazon clouds with Oceanic systems during the wet season

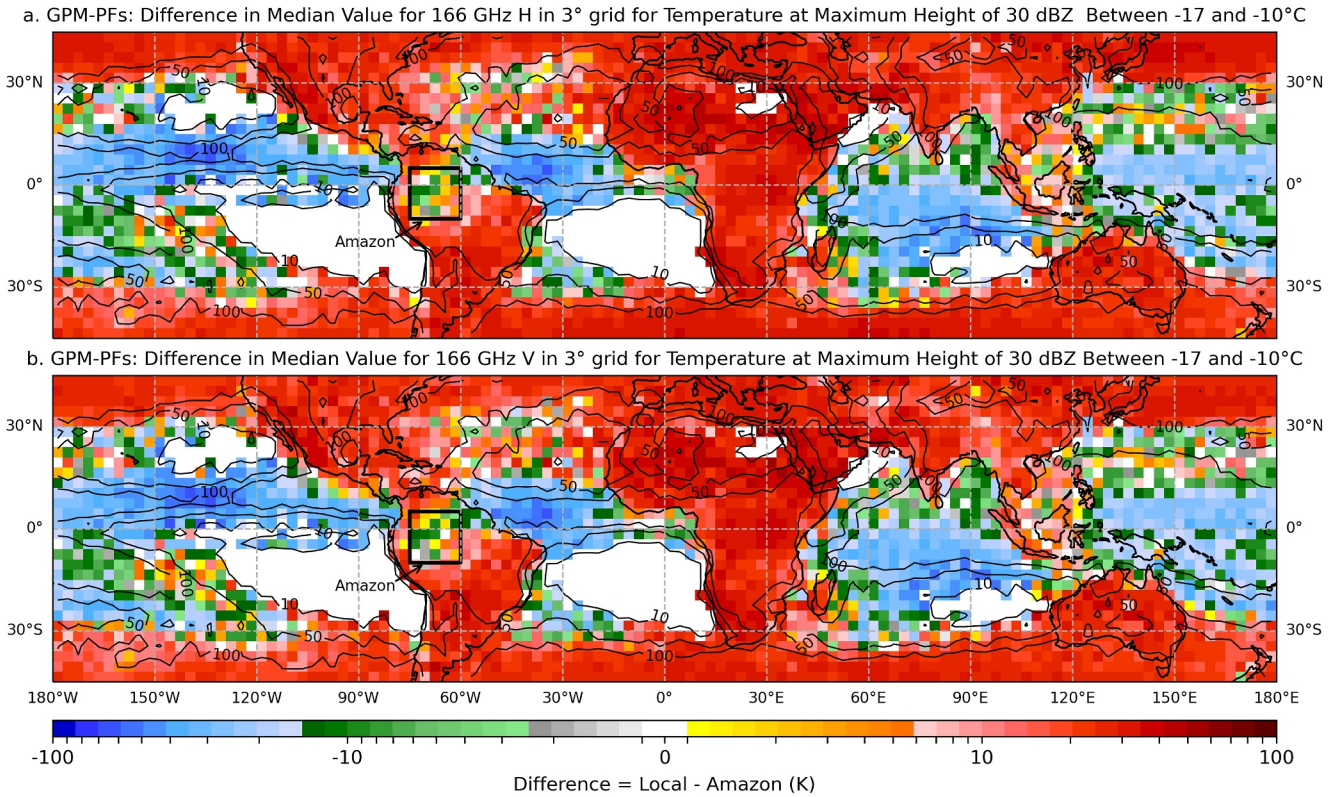

Figure 8. Same as Figure 7, except for (a) 166 GHz Horizontal, and (b) 166 GHz Vertical.

(January-March; i.e., 3 months), while the data analyzed in this study include full-years. The 15 × 15° AM box appears as an in-between state, passive-microwave wise, between land and ocean systems.

It is noteworthy to mention that at 85/89 GHz and high frequencies, the earth surface background is totally absorbed by the thick layer of liquid water in the lower layers of the clouds (Ellison, 2007; Rosenkranz, 2014). Upwelling microwave radiation at these frequencies is consequently reduced to the weaker upward component of re-emitted signal. The upward component of this signal, produced by the lower parts of the cloud, will then be scattered by particles whose size approximates the wavelength (i.e., hail for 37 GHz with a wavelength of approximately 0.81 cm; and small ice particles for 85/89 GHz with a wavelength of approximately 0.35–0.34 cm). Additionally, Mushtak et al. (2005) show that the mean cloud base height increases with latitude (Mushtak et al., 2005, Figure 5) while the altitude of the 0°C isotherm decreases. It implies that the layer of liquid water within a cloud tends to be narrower at higher latitudes than it is in the tropics. This could lead to a reduced emission from the liquid phase and result in a lower TB. However, Figures 6–9 show high positive values (i.e., increase of the TB) in the difference in medians observed at high latitudes (i.e., above 30° of absolute latitude) for channels at, and above 85/89 GHz. This can be explained by the shallower depth of the layer of ice precipitation in the mid-high latitudes. The thickness of the ice precipitation layer above freezing level for PFs with T_{30dBZ} between −17°C and −10°C are computed as the maximum radar echo top height minus the altitude of the freezing level obtained from ERA5 and are shown as an average in Figure 10. The thickness of the ice precipitation layer is well correlated with the increase of the median TB values at high latitudes at these frequencies. A thinner ice precipitation layer, as it would translate into a smaller quantity in ice water path on average, would result in a weaker scattering of the upward radiance, leading to higher TB values for frequencies at 85/89 GHz and higher, and leading to lower TB values at 37 GHz.

Additionally, Figure 10 emphasizes the "Green Ocean" aspect of the Amazon. For example, comparing areas of similar latitude in either TRMM (Figure 10a) or GPM (Figure 10b) shows that the Amazon appears to have a thicker ice precipitation layer (i.e., averaging 5–6 km) compared to other land areas (e.g., Central Africa averages 4–5 km), but remains thinner than oceanic areas (e.g., averaging 5–7 km). Although not being the main focus of

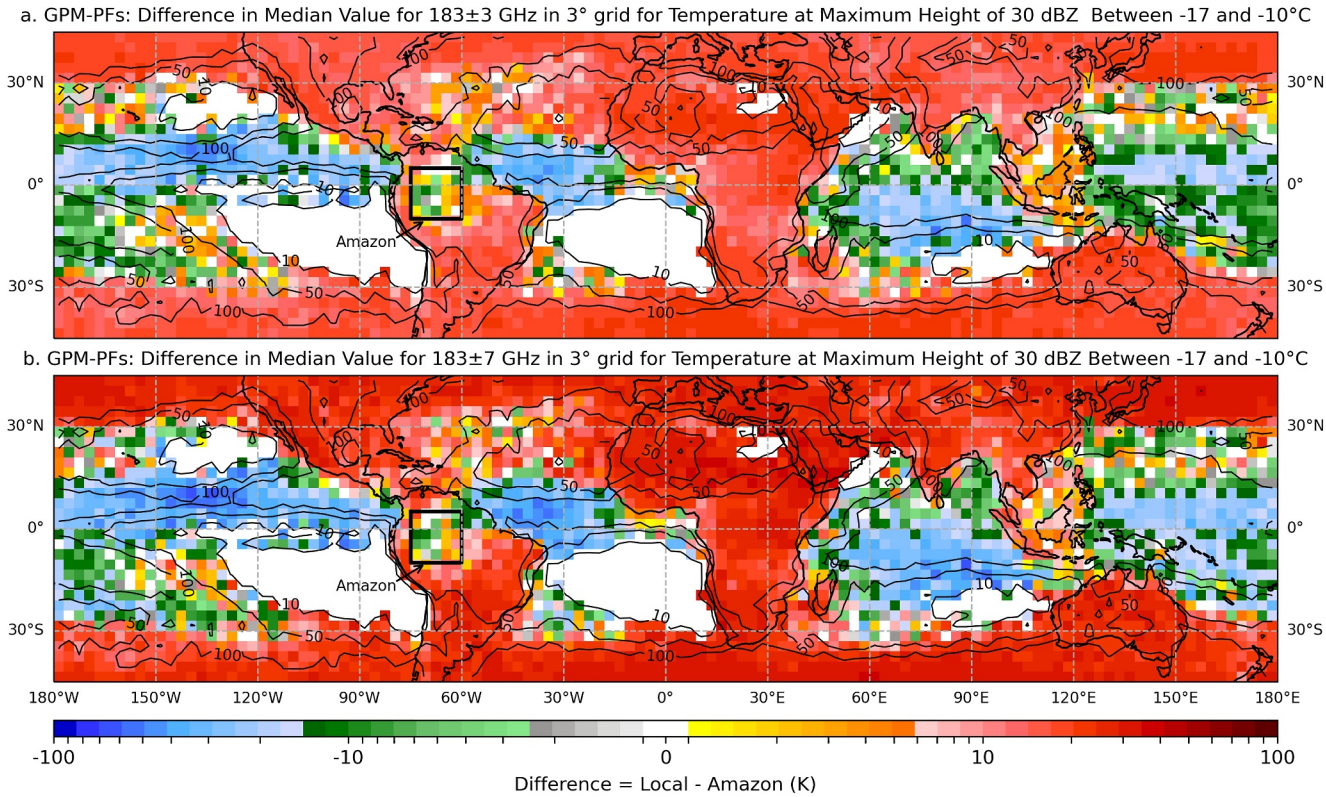

Figure 9. Same as Figure 7, except for (a) 183 ± 3 GHz, and (b) 183 ± 7 GHz.

this figure, it follows the theory studied in this paper regarding the oceanic-like ice composition of Amazonian PFs (i.e., smaller but more numerous ice crystals). Note that this ice precipitation thickness is different from the ice cloud depth as the true cloud top height is higher than the maximum height measured with the precipitation radar through the detectable signal around 12–18 dBZ (Hamada & Takayabu, 2016). It consequently corresponds to a slight underestimation of the ice cloud depth. However, oceanic systems usually have lower vertical gradience in reflectivity profiles than their overland homologs in the ice regime (Zipser & Lutz, 1994), for the same reason of smaller ice particles, meaning that the cloud top altitude could be further above the echo top in such systems (Liu et al., 2007).

Note that the ice precipitation layer thickness computed for TRMM is lower than for GPM as a result of the lower sensitivity compared to the one onboard GPM, allowing GPM's DPR to observe weaker convection pockets reaching higher altitudes.

Interestingly, both TRMM-LPFs and GPM-PFs show that the median TB value of PFs in AM is closer in value to the median TB observed in the most electrically active areas of the Oceans (Figure 1a, with a $\log_{10}$ scale), including the South Pacific Convergence Zone (SPCZ) and tropical west Pacific off the equator. It implies that PFs over these ocean regions have relatively warm TBs and contain some large ice particles for a given 30 dBZ echo top height, therefore, more likely to have lightning.

Table 2
Median Brightness Temperature Measured in Amazonian PFs With a Temperature at Maximum 30 dBZ Echo Top Height Between −17°C and −10°C for Each Channel of TRMM-MI and GPM-MI

		Channel frequency (GHz)					
		37 PCT	85/89 PCT	166 H	166 V	183 ± 3	183 ± 7
Median TB (K)	TRMM-LPFs	276.25	236.56				
	GPM-PFs	275.30	243.28	207.65	212.77	231.43	220.11

Table 3
Proportions of TRMM-PFs With Temperature at 30 dBZ Echo Top (T_{30dBZ}) Around −10°C Over Land and −17°C Over Ocean Within TRMM Domain and in Tropics

	Proportion of TRMM-PFs having lightning			
	Land		Oceans	
	$-11°C \leq T_{30dBZ} \leq -9°C$	$T_{30dBZ} \leq -10°C$	$-18°C \leq T_{30dBZ} \leq -16°C$	$T_{30dBZ} \leq -17°C$
Total (36°S–36°N)	7.51%	47.29%	7.53%	15.18%
Tropics (20°S–20°N)	7.81%	52.06%	7.80%	15.82%

4. Summary

Using the Precipitation Features data sets from TRMM and GPM, comparisons are made between thunderstorms produced in the Amazonian region and the ones produced in the Congo Basin. By examining the systems with similar radar reflectivity properties, this study shows evidence of ice microphysics differences that could explain the differences in lightning activity between the two regions. The major findings include:

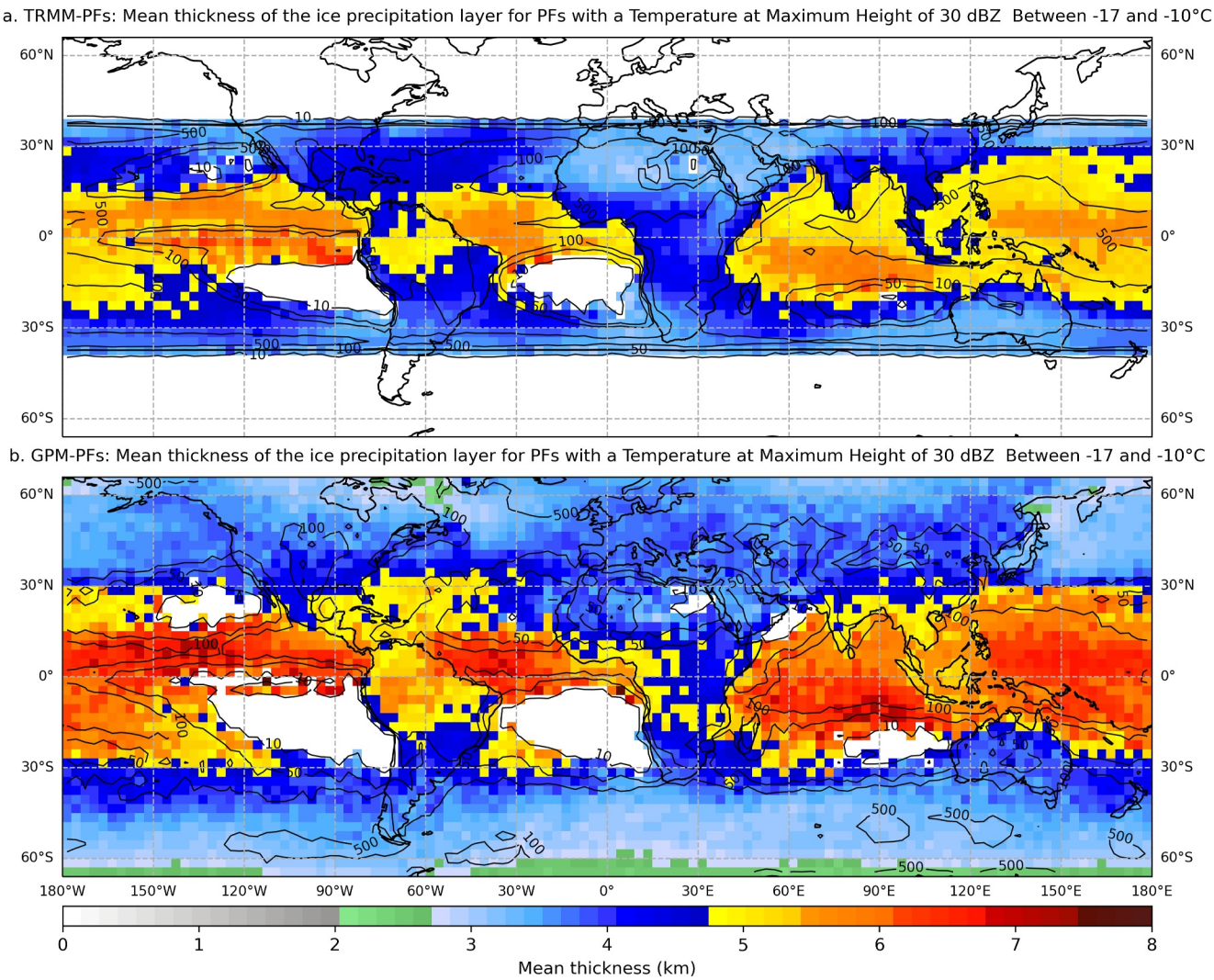

Figure 10. Average thickness of the ice precipitation layer of PFs with T_{30dBZ} between −17°C and −10°C on 3 × 3° grid for (a) TRMM (1998–2013), and (b) GPM (2015–2021). Thickness is computed as the maximum radar echo top height (TRMM-PR and GPM-DPR) minus the altitude of the freezing level (ERA5). Sample size is presented by the black contours.

- The maximum reflectivity profiles in thunderstorms over the Amazon show a narrower distribution than those in the Congo Basin, which have maximum reflectivity values up to 15 dB higher.
- For two thunderstorms with the same ice water content or area of 30 dBZ at −10°C, the thunderstorm over the Congo Basin produces on average up to twice as many lightning flashes than the Amazonian one. This flash count difference is quantified and increases with systems size or ice water content.
- For a system with a same maximum echo top height of 30 dBZ, the brightness temperature tends to be lower for the Amazon at 85/89, 166, and 183 GHz, but tends to be higher at 37 GHz compared to Congo Basin.

With the intensity of the reflectivity being driven by size (to the sixth power) and quantity of hydrometeors, it implies that higher reflectivity values in Congo Basin are driven by large ice particle sizes, while the narrowly distributed lower reflectivity values in Amazon implies numerous smaller ice particles. This is consistent with the fewer lightning counts observed in Amazonian PFs. Because lightning count is a function of ice hydrometeor collisions (i.e., charges separation is driven by large hydrometeors) and area of charge (i.e., a wider charging area is bound to produce more lightning strikes), precipitation features in AM and CG with similar values of IWC or A_{charge} should have similar flash counts, unless their microphysics is significantly different. Microwave brightness temperatures show that Amazonian PFs indeed produce less hail with warmer TBs at 37 GHz, but it also shows that they produce a higher frozen precipitations content with colder TBs at frequencies higher than 85/89 GHz.

Next, a comparison of the median brightness temperatures of PFs with a temperature at the echo top height of 30 dBZ between −17°C and −10°C (marginally suggestive of thunderstorm activity; Liu et al. (2010)) is made between the Amazonian rain forest and the rest of the world. Results show that:

- The convective systems in the Amazon have lower TBs and relatively smaller ice particles than most land regions, except Maritime continents, but have warmer TBs than oceans.
- Amazonian PFs present similar TB values compared to some specific oceanic areas (e.g., SPCZ and west Pacific off the equator) which are correlated with a higher oceanic lightning activity. This implies that over these regions, convection is relatively stronger than the rest of the oceans, with larger ice particles to help producing lightning.
- PFs over the Amazonian rain forest are shown to present brightness temperature values corresponding to neither land nor oceans, it can be assimilated as an in-between region, assumed to result from the maritime-like systems produced over land during the wet-season (i.e., "Green Ocean").

The different regimes happening within the Amazonian rain forest (i.e., during the wet season vs. the remaining months) have not been further explored in this study.

Data Availability Statement

All data sets used in this study are freely and openly available. The ERA5 data is available at https://cds.climate.copernicus.eu/ (Hersbach et al., 2023). The TRMM and GPM Precipitation Features databases are available at http://atmos.tamucc.edu/trmm/data/.

Acknowledgments
We would like to thank Daniel Cecil, Sarah Bang, and an anonymous reviewer for their valuable comments. This research was supported by NASA PMM program under Grant 80NSSC22K0591 and NSF-AGS-2219639. Thanks to the Precipitation Processing System (PPS) team at NASA Goddard Space Flight Center, Greenbelt, MD, for data processing assistance.

References

Adler, R. F., Yeh, H. Y. M., Prasad, N., Tao, W. K., & Simpson, J. (1991). Microwave simulations of a tropical rainfall system with a three-dimensional cloud model. *Journal of Applied Meteorology and Climatology*, *30*(7), 924–953. https://doi.org/10.1175/1520-0450-30.7.924

Albrecht, R. I., Goodman, S. J., Buechler, D. E., Blakeslee, R. J., & Christian, H. J. (2016). Where are the lightning hotspots on Earth? *Bulletin of the American Meteorological Society*, *97*(11), 2051–2068. https://doi.org/10.1175/bams-d-14-00193.1

Albrecht, R. I., Goodman, S. J., Petersen, W. A., Buechler, D. E., Bruning, E. C., Blakeslee, R. J., & Christian, H. J. (2011). The 13 years of TRMM Lightning Imaging Sensor: From individual flash characteristics to decadal tendencies. In *XIV ICAE: International Conference on atmospheric Electricity (No. M11-0203)*.

Allen, J. T., Giammanco, I. M., Kumjian, M. R., Jurgen Punge, H., Zhang, Q., Groenemeijer, P., et al. (2020). Understanding hail in the earth system. *Reviews of Geophysics*, *58*(1), e2019RG000665. https://doi.org/10.1029/2019rg000665

Bang, S. D., & Cecil, D. J. (2019). Constructing a multifrequency passive microwave hail retrieval and climatology in the GPM domain. *Journal of Applied Meteorology and Climatology*, *58*(9), 1889–1904. https://doi.org/10.1175/jamc-d-19-0042.1

Bang, S. D., & Cecil, D. J. (2021). Testing passive microwave-based hail retrievals using GPM DPR Ku-band radar. *Journal of Applied Meteorology and Climatology*, *60*(3), 255–271. https://doi.org/10.1175/jamc-d-20-0129.1

Bennartz, R., & Bauer, P. (2003). Sensitivity of microwave radiances at 85–183 GHz to precipitating ice particles. *Radio Science*, *38*(4), 40–41. https://doi.org/10.1029/2002rs002626

Blakeslee, R. J., Lang, T. J., Koshak, W. J., Buechler, D., Gatlin, P., Mach, D. M., et al. (2020). Three years of the lightning imaging sensor onboard the international space station: Expanded global coverage and enhanced applications. *Journal of Geophysical Research: Atmospheres*, *125*(16), e2020JD032918. https://doi.org/10.1029/2020jd032918

Boccippio, D. J., Cummins, K. L., Christian, H. J., & Goodman, S. J. (2001). Combined satellite-and surface-based estimation of the intracloud–cloud-to-ground lightning ratio over the continental United States. *Monthly Weather Review*, *129*(1), 108–122. https://doi.org/10.1175/1520-0493(2001)129<0108:csasbe>2.0.co;2

Boccippio, D. J., Goodman, S. J., & Heckman, S. (2000). Regional differences in tropical lightning distributions. *Journal of Applied Meteorology and Climatology*, *39*(12), 2231–2248. https://doi.org/10.1175/1520-0450(2001)040<2231:rditld>2.0.co;2

Boccippio, D. J., Koshak, W., Blakeslee, R., Driscoll, K., Mach, D., Buechler, D., et al. (2000). The optical transient detector (OTD): Instrument characteristics and cross-sensor validation. *Journal of Atmospheric and Oceanic Technology*, *17*(4), 441–458. https://doi.org/10.1175/1520-0426(2000)017<0441:totdoi>2.0.co;2

Brook, J. P., Soderholm, J. S., Protat, A., McGowan, H., & Warren, R. A. (2024). A radar-based hail climatology of Australia. *Monthly Weather Review*, *152*(2), 607–628. https://doi.org/10.1175/mwr-d-23-0130.1

Carey, L. D., & Rutledge, S. A. (2000). The relationship between precipitation and lightning in tropical island convection: A C-band polarimetric radar study. *Monthly Weather Review*, *128*(8), 2687–2710. https://doi.org/10.1175/1520-0493(2000)128<2687:trbpal>2.0.co;2

Cecil, D. J. (2009). Passive microwave brightness temperatures as proxies for hailstorms. *Journal of Applied Meteorology and Climatology*, *48*(6), 1281–1286. https://doi.org/10.1175/2009jamc2125.1

Cecil, D. J., Buechler, D. E., & Blakeslee, R. J. (2014). Gridded lightning climatology from TRMM-LIS and OTD: Dataset description. *Atmospheric Research*, *135*, 404–414. https://doi.org/10.1016/j.atmosres.2012.06.028

Cecil, D. J., Buechler, D. E., & Blakeslee, R. J. (2015). TRMM LIS climatology of thunderstorm occurrence and conditional lightning flash rates. *Journal of Climate*, *28*(16), 6536–6547. https://doi.org/10.1175/jcli-d-15-0124.1

Cecil, D. J., & Chronis, T. (2018). Polarization-corrected temperatures for 10-19-37-and 89-GHz passive microwave frequencies. *Journal of Applied Meteorology and Climatology*, *57*(10), 2249–2265. https://doi.org/10.1175/JAMC-D-18-0022.1

Cecil, D. J., Goodman, S. J., Boccippio, D. J., Zipser, E. J., & Nesbitt, S. W. (2005). Three years of TRMM precipitation features. Part I: Radar, radiometric, and lightning characteristics. *Monthly Weather Review*, *133*(3), 543–566. https://doi.org/10.1175/mwr-2876.1

Cecil, D. J., Zipser, E. J., & Nesbitt, S. W. (2002). Reflectivity, ice scattering, and lightning characteristics of hurricane eyewalls and rainbands. Part I: Quantitative description. *Monthly Weather Review*, *130*(4), 769–784. https://doi.org/10.1175/1520-0493(2002)130<0769:risalc>2.0.co;2

Christian, H. J. (1999). Optical detection of lightning from space. In *11th International Conference on Atmospheric Electricity*.

Christian, H. J., Blakeslee, R. J., Boccippio, D. J., Boeck, W. L., Buechler, D. E., Driscoll, K. T., et al. (2003). Global frequency and distribution of lightning as observed from space by the Optical Transient Detector. *Journal of Geophysical Research*, *108*(D1), ACL–4. https://doi.org/10.1029/2002jd002347

Deierling, E., & Petersen, W. A. (2008). Total lightning activity as an indicator of updraft characteristics. *Journal of Geophysical Research*, *113*(D16). https://doi.org/10.1029/2007JD009598

Deierling, W., Petersen, W. A., Latham, J., Ellis, S., & Christian, H. J. (2008). The relationship between lightning activity and ice fluxes in thunderstorms. *Journal of Geophysical Research*, *113*(D15), D15210. https://doi.org/10.1029/2007JD009700

Ellison, W. J. (2007). Permittivity of pure water, at standard atmospheric pressure, over the frequency range–25THz and the temperature range–100°C. *Journal of Physical and Chemical Reference Data*, *36*(1), 1–18. https://doi.org/10.1063/1.2360986

Futyan, J. M., & Del Genio, A. D. (2007). Relationships between lightning and properties of convective cloud clusters. *Geophysical Research Letters*, *34*(15). https://doi.org/10.1029/2007gl030227

Gaskell, W. (1981). A laboratory study of the inductive theory of thunderstorm electrification. *Quarterly Journal of the Royal Meteorological Society*, *107*(454), 955–966. https://doi.org/10.1256/smsqj.45412

Hamada, A., & Takayabu, Y. N. (2016). Improvements in detection of light precipitation with the Global Precipitation Measurement dual-frequency precipitation radar (GPM DPR). *Journal of Atmospheric and Oceanic Technology*, *33*(4), 653–667. https://doi.org/10.1175/JTECH-D-15-0097.1

Hersbach, H., Bell, B., Berrisford, P., Biavati, G., Horányi, A., Muñoz Sabater, J., et al. (2023). ERA5 hourly data on single levels from 1940 to present [Dataset]. *Copernicus Climate Change Service (C3S) Climate Data Store (CDS)*. https://doi.org/10.24381/cds.adbb2d47

Hersbach, H., Bell, B., Berrisford, P., Hirahara, S., Horányi, A., Muñoz-Sabater, J., et al. (2020). The ERA5 global reanalysis. *Quarterly Journal of the Royal Meteorological Society*, *146*(730), 1999–2049. https://doi.org/10.1002/qj.3803

Heuscher, L., Liu, C., Gatlin, P., & Petersen, W. A. (2022). Relationship between lightning, precipitation, and environmental characteristics at mid-/high latitudes from a GLM and GPM perspective. *Journal of Geophysical Research: Atmospheres*, *127*(13), e2022JD036894. https://doi.org/10.1029/2022jd036894

Laksen, H. R., & Stansbury, E. J. (1974). Association of lightning flashes with precipitation cores extending to height 7 km. *Journal of Atmospheric and Terrestrial Physics*, *36*(9), 1547–1553. https://doi.org/10.1016/0021-9169(74)90232-3

Le, M., & Chandrasekar, V. (2021). Graupel and hail identification algorithm for the dual-frequency precipitation radar (DPR) on the GPM core satellite. *Journal of the Meteorological Society of Japan. Ser. II*, *99*(1), 49–65. https://doi.org/10.2151/jmsj.2021-003

Leppert, K. D., & Cecil, D. J. (2015). Signatures of hydrometeor species from airborne passive microwave data for frequencies 10–183 GHz. *Journal of Applied Meteorology and Climatology*, *54*(6), 1313–1334. https://doi.org/10.1175/jamc-d-14-0145.1

Leppert II, K. D., & Cecil, D. J. (2019). Sensitivity of simulated GMI brightness temperatures to variations in particle size distributions in a severe hailstorm. *Journal of Applied Meteorology and Climatology*, *58*(9), 1905–1930. https://doi.org/10.1175/jamc-d-19-0031.1

Liu, C., Cecil, D., & Zipser, E. J. (2011). Relationships between lightning flash rates and passive microwave brightness temperatures at 85 and 37 GHz over the tropics and subtropics. *Journal of Geophysical Research*, *116*(D23). https://doi.org/10.1029/2011jd016463

Liu, C., Cecil, D. J., Zipser, E. J., Kronfeld, K., & Robertson, R. (2012). Relationships between lightning flash rates and radar reflectivity vertical structures in thunderstorms over the tropics and subtropics. *Journal of Geophysical Research*, *117*(D6). https://doi.org/10.1029/2011jd017123

Liu, C., Williams, E. R., Zipser, E. J., & Burns, G. (2010). Diurnal variations of global thunderstorms and electrified shower clouds and their contribution to the global electrical circuit. *Journal of the Atmospheric Sciences*, *67*(2), 309–323. https://doi.org/10.1175/2009jas3248.1

Liu, C., Zipser, E., & Nesbitt, S. W. (2007). Global distribution of tropical deep convection: Different perspectives using infrared and radar as the primary data source. *Journal of Climate*, *20*(3), 489–503. https://doi.org/10.1175/jcli4023.1

Liu, C., Zipser, E. J., Cecil, D. J., Nesbitt, S. W., & Sherwood, S. (2008). A cloud and precipitation feature database from nine years of TRMM observations. *Journal of Applied Meteorology and Climatology*, *47*(10), 2712–2728. https://doi.org/10.1175/2008jamc1890.1

McCollum, J. R., Gruber, A., & Ba, M. B. (2000). Discrepancy between gauges and satellite estimates of rainfall in equatorial Africa. *Journal of Applied Meteorology and Climatology*, *39*(5), 666–679. https://doi.org/10.1175/1520-0450-39.5.666

Mech, M., Crewell, S., Meirold-Mautner, I., Prigent, C., & Chaboureau, J. P. (2007). Information content of millimeter-wave observations for hydrometeor properties in mid-latitudes. *IEEE Transactions on Geoscience and Remote Sensing*, *45*(7), 2287–2299. https://doi.org/10.1109/tgrs.2007.898261

Michele, S. D., & Bauer, P. (2006). Passive microwave radiometer channel selection basedoncloud and precipitation information content. *Quarterly Journal of the Royal Meteorological Society: A Journal of the Atmospheric Sciences, Applied Meteorology and Physical Oceanography*, *132*(617), 1299–1323. https://doi.org/10.1256/qj.05.164

Mohr, K. I., Famiglietti, J. S., & Zipser, E. J. (1999). The contribution to tropical rainfall with respect to convective system type, size, and intensity estimated from the 85-GHz ice-scattering signature. *Journal of Applied Meteorology and Climatology*, *38*(5), 596–606. https://doi.org/10.1175/1520-0450(1999)038<0596:tcttrw>2.0.co;2

Morvais, F., & Liu, C. (2023). Estimation of lightning flash rate in precipitation features by applying shallow AI neural network models to the GMI passive microwave brightness temperatures. *Journal of Geophysical Research: Atmospheres*, *128*(23), e2023JD039516. https://doi.org/10.1029/2023jd039516

Mroz, K., Battaglia, A., Lang, T. J., Cecil, D. J., Tanelli, S., & Tridon, F. (2017). Hail-detection algorithm for the GPM Core Observatory satellite sensors. *Journal of Applied Meteorology and Climatology*, *56*(7), 1939–1957. https://doi.org/10.1175/jamc-d-16-0368.1

Murphy, M. J., & Nag, A. (2015). Cloud lightning performance and climatology of the US based on the upgraded US National Lightning Detection Network. In *Seventh Conf. On the Meteorological Applications of Lightning Data*.

Mushtak, V. C., Williams, E. R., & Boccippio, D. J. (2005). Latitudinal variations of cloud base height and lightning parameters in the tropics. *Atmospheric Research*, *76*(1–4), 222–230. https://doi.org/10.1016/j.atmosres.2004.11.010

Nesbitt, S. W., Zipser, E. J., & Cecil, D. J. (2000). A census of precipitation features in the tropics using TRMM: Radar, ice scattering, and lightning observations. *Journal of Climate*, *13*(23), 4087–4106. https://doi.org/10.1175/1520-0442(2000)013<4087:acopfi>2.0.co;2

Orville, R. E., & Spencer, D. W. (1979). Global lightning flash frequency. *Monthly Weather Review*, *107*(7), 934–943. https://doi.org/10.1175/1520-0493(1979)107<0934:glff>2.0.co;2

Pechony, O., & Nickolaenko, A. (2010). The South American lightning puzzle and the South Atlantic anomaly. *Journal of Atmospheric Electricity*, *30*(2), 75–82. https://doi.org/10.1541/jae.30.75

Petersen, W. A., Christian, H. J., & Rutledge, S. A. (2005). TRMM observations of the global relationship between ice water content and lightning. *Geophysical Research Letters*, *32*(14). https://doi.org/10.1029/2005gl023236

Petersen, W. A., & Rutledge, S. A. (2001). Regional variability in tropical convection: Observations from TRMM. *Journal of Climate*, *14*(17), 3566–3586. https://doi.org/10.1175/1520-0442(2001)014<3566:rvitco>2.0.co;2

Peterson, M., & Liu, C. (2011). Global statistics of lightning in anvil and stratiform regions over the tropics and subtropics observed by the Tropical Rainfall Measuring Mission. *Journal of Geophysical Research*, *116*(D23), D23201. https://doi.org/10.1029/2011JD015908

Racette, P. E., Westwater, E. R., Han, Y., Gasiewski, A. J., Klein, M., Cimini, D., et al. (2005). Measurement of low amounts of precipitable water vapor using ground-based millimeterwave radiometry. *Journal of Atmospheric and Oceanic Technology*, *22*(4), 317–337. https://doi.org/10.1175/jtech1711.1

Rosenkranz, P. W. (2014). A model for the complex dielectric constant of supercooled liquid water at microwave frequencies. *IEEE Transactions on Geoscience and Remote Sensing*, *53*(3), 1387–1393. https://doi.org/10.1109/tgrs.2014.2339015

Saunders, C. (2008). Charge separation mechanisms in clouds. *Planetary Atmospheric Electricity*, *137*(1–4), 335–353. https://doi.org/10.1007/s11214-008-9345-0

Saunders, C. P. R., & Peck, S. L. (1998). Laboratory studies of the influence of the rime accretion rate on charge transfer during crystal/graupel collisions. *Journal of Geophysical Research*, *103*(D12), 13949–13956. https://doi.org/10.1029/97jd02644

Smith, E. A., Cooper, H. J., Xiang, X., Mugnai, A., & Tripoli, G. J. (1992). Foundations for statistical-physical precipitation retrieval from passive microwave satellite measurements. Part I: Brightness-temperature properties of a time-dependent cloud-radiation model. *Journal of Applied Meteorology and Climatology*, *31*(6), 506–531. https://doi.org/10.1175/1520-0450(1992)031<0506:ffsppr>2.0.co;2

Spencer, R. W., Goodman, H. M., & Hood, R. E. (1989). Precipitation retrieval over land and ocean with the SSM/I: Identification and characteristics of the scattering signal. *Journal of Atmospheric and Oceanic Technology*, *6*(2), 254–273. https://doi.org/10.1175/1520-0426(1989)006<0254:prolao>2.0.co;2

Takahashi, T. (1978). Riming electrification as a charge generation mechanism in thunderstorms. *Journal of the Atmospheric Sciences*, *35*(8), 1536–1548. https://doi.org/10.1175/1520-0469(1978)035<1536:reaacg>2.0.co;2

Toracinta, E. R., Cecil, D. J., Zipser, E. J., & Nesbitt, S. W. (2002). Radar, passive microwave, and lightning characteristics of precipitating systems in the tropics. *Monthly Weather Review*, *130*(4), 802–824. https://doi.org/10.1175/1520-0493(2002)130<0802:rpmalc>2.0.co;2

Toracinta, E. R., Mohr, K. I., Zipser, E. J., & Orville, R. E. (1996). A comparison of WSR-88D reflectivities, SSM/I brightness temperatures, and lightning for mesoscale convective systems in Texas. Part I: Radar reflectivity and lightning. *Journal of Applied Meteorology and Climatology*, *35*(6), 902–918. https://doi.org/10.1175/1520-0450(1996)035<0902:acowrs>2.0.co;2

Vivekanandan, J., Turk, J., & Bringi, V. N. (1991). Ice water path estimation and characterization using passive microwave radiometry. *Journal of Applied Meteorology and Climatology*, *30*(10), 1407–1421. https://doi.org/10.1175/1520-0450(1991)030<1407:iwpeac>2.0.co;2

Wexler, R., & Swingle, D. M. (1947). Radar storm detection. *Bulletin of the American Meteorological Society*, *28*(4), 159–167. https://doi.org/10.1175/1520-0477-28.4.159

Wilheit, T. T., Hobbs, P. V., Jin, K., Rangno, A. L., Triesky, M. E., & Wang, J. R. (2006). Microwave radiative transfer in the mixed-phase regions of tropical rainfall. *Journal of Atmospheric and Oceanic Technology*, *23*(11), 1519–1529. https://doi.org/10.1175/jtech1944.1

Williams, E., Rosenfeld, D., Madden, N., Gerlach, J., Gears, N., Atkinson, L., et al. (2002). Contrasting convective regimes over the Amazon: Implications for cloud electrification. *Journal of Geophysical Research*, *107*(D20), LBA–50. https://doi.org/10.1029/2001jd000380

Williams, E., & Stanfill, S. (2002). The physical origin of the land–ocean contrast in lightning activity. *Comptes Rendus Physique*, *3*(10), 1277–1292. https://doi.org/10.1016/s1631-0705(02)01407-x

Williams, E. R. (2005). Lightning and climate: A review. *Atmospheric Research*, *76*(1–4), 272–287. https://doi.org/10.1016/j.atmosres.2004.11.014

Williams, E. R., & Sátori, G. (2004). Lightning, thermodynamic and hydrological comparison of the two tropical continental chimneys. *Journal of Atmospheric and Solar-Terrestrial Physics*, *66*(13–14), 1213–1231. https://doi.org/10.1016/j.jastp.2004.05.015

Wu, M. L. C. (1987). Determination of cloud ice water content and geometrical thickness using microwave and infrared radiometric measurements. *Journal of Climate and Applied Meteorology*, *26*(8), 878–884. https://doi.org/10.1175/1520-0450(1987)026<0878:dociwc>2.0.co;2

Zipser, E. J. (1994). Deep cumulonimbus cloud systems in the tropics with and without lightning. *Monthly Weather Review*, *122*(8), 1837–1851. https://doi.org/10.1175/1520-0493

Zipser, E. J., Cecil, D. J., Liu, C., Nesbitt, S. W., & Yorty, D. P. (2006). Where are the most intense thunderstorms on Earth? *Bulletin of the American Meteorological Society*, *87*(8), 1057–1072. https://doi.org/10.1175/bams-87-8-1057

Zipser, E. J., & Lutz, K. R. (1994). The vertical profile of radar reflectivity of convective cells: A strong indicator of storm intensity and lightning probability? *Monthly Weather Review*, *122*(8), 1751–1759. https://doi.org/10.1175/1520-0493(1994)122<1751:tvporr>2.0.co;2